RC 20101 (06/15/95)
Engineering and Technology

IBM Research Report

On Particle–Mesh Coupling in Monte Carlo Semiconductor Device Simulation

S.E. Laux

IBM Research Division
T.J. Watson Research Center
Yorktown Heights, New York

IBM Research Division
Almaden · T.J. Watson · Tokyo · Zurich

On Particle–Mesh Coupling in Monte Carlo Semiconductor Device Simulation*

S.E. Laux
IBM Research Division; T.J. Watson Research Center
P.O Box 218; Yorktown Heights, NY 10598 USA

Improved nearest-grid-point and cloud-in-cell particle-mesh schemes are suggested, and a new nearest-element-center scheme proposed, to help reduce self force and improve the spatial accuracy of forces in Monte Carlo semiconductor device simulation. These schemes are exercised on both one- and two-dimensional model problems. An attempt to design a scheme with reduced self force for unstructured triangular meshes is unsuccessful.

1 Introduction

A proper coupling between charged particles and Coulombic forces is required to maintain zero self force and spatial accuracy of forces in self-consistent Monte Carlo device modeling. These issues have been dealt with at length by Hockney and Eastwood[1]. The charge assignment and force interpolation schemes usually employed in self-consistent Monte Carlo device simulation are the nearest-grid-point (NGP) or cloud-in-cell (CIC) schemes[1]. These schemes may be used in semiconductor simulation, subject to the following two restrictions: (P) permittivity must be constant, and (M) a tensor product mesh with uniform spacing in each axis direction must be employed. If these restrictions are ignored, self force becomes nonzero and/or spatial accuracy of forces is sacrificed. The two concepts are related. Self force refers to the force a charge may exert *upon itself* in an idealized situation, namely, a lone charge sitting in a domain of infinite extent and constant permittivity. Physically, this lone charge should experience no force; numerically, any force experienced is self force[1]. Spatial accuracy of forces is a broader term, referring to the extent all forces acting upon a charge are correctly resolved in a realistic context. The first step to obtaining good spatial

*Portions of this paper were presented at the Sixth Int. Conf. on Simulation of Semiconductor Devices and Processes (SISDEP'95), Erlangen, Germany, September 6-8, 1995.

accuracy of forces is to insure the self force is zero. The NGP and CIC schemes do just this; however, restrictions (P) and (M) severely limit the scope of devices that may be considered in device simulation. This paper proposes new particle-mesh (PM) coupling schemes which relax, or remove, these restrictions while maintaining small self force and good spatial accuracy.

Given the above two restrictions, it may seem natural to pursue different schemes to obtain the self-consistent forces between the charged particles in the device domain. Two such schemes are a molecular dynamics approach[2] or a multipole expansion method[3]. Unfortunately, the former approach has yet to be demonstrated in all but the simplest geometries, and never in geometries containing spatially dependent permittivity. The latter approach has been applied to situations of spatially dependent permittivity, but only for the Laplace equation. Thus, neither approach has demonstrated the necessary generality required for semiconductor device simulation.

After a general discussion of PM coupling, this paper describes improvements to the NGP and CIC charge assignment/force interpolation schemes which do not require restriction (P) above, and a new nearest-element-center (NEC) scheme which, in addition, relaxes restriction (M). The characteristics of the NEC scheme will be examined in detail. Finally, this leads naturally to a discussion of designing a scheme for unstructured triangular meshes, which remains an open question.

2 Particle-Mesh Coupling

PM coupling can be broken into four steps[1]: (i) assign particle charge to the mesh; (ii) solve the Poisson equation on the mesh; (iii) calculate the mesh-defined forces; and (iv) interpolate to find forces on the particles. These steps will be revisited throughout this paper as new PM schemes are proposed.

While spatial accuracy of forces is always of importance, discussing self force is only relevant if the Coulombic forces are obtained self-consistently in time with particle position. Such a computation would be capable of performing a true transient device simulation, for example. Any smoothing of the electric field in time (*e.g.*, [4]) or using a time-invariant ("frozen") field (*e.g.*, [5]) renders a discussion of self force irrelevant, as the force does not track instantaneous particle motion.

In its simplest embodiment, self force arises due to the failure of a non-uniformly spaced mesh to resolve symmetrically the potential singularity of a single charge (in 2D, a line charge). Differencing this potential and interpolating back to the charge position yields an erroneous, non-zero force exerted by the charge upon "itself". But note, self forces may be small locally compared to the total force. Self force is expected to be most serious in regions of a device where doping is "high", and hence, internal fields are "low". In MOSFET channels, for example, local fields are probably dominated by the field attributable to gate and/or drain biases. Of what order of magnitude is self force? As a crude estimate, at a distance L from a line charge of linear number density $\mathcal{S}$, the force F_s is

$$F_s = \frac{q\mathcal{S}}{2\pi\epsilon L} = 24,600 \left(\frac{\mathcal{S}}{10^5 \text{ cm}^{-1}}\right)\left(\frac{L}{10^{-7} \text{ cm}}\right) \qquad \text{eV/cm}\,, \tag{1}$$

where the normalizations for $\mathcal{S}$ and L are typical of the line charge magnitude and mesh spacing for a two-dimensional device simulation. F_s can indeed be significant when internals fields are "low".

This paper assumes two-dimensional device simulation, although the extension to three dimensions carries over in an obvious way. Some one-dimensional examples are included as well, to help clarify ideas. "Force" and "electric field" acting on a charge are used interchangeably throughout this paper, being proportional to each other by the charge of the particle. Force has the advantage of always denoting the direction a charge will be accelerated, independent of the polarity of the charge.

3 Improved NGP/CIC and the NEC Scheme

Before discussing the improved NGP/CIC and the new NEC schemes, the standard NGP and CIC schemes[1] are first briefly reviewed to establish notation. Consider a tensor product mesh with meshlines x_i, $i = 1, \ldots, \mathcal{N}_x$ and y_j, $j = 1, \ldots, \mathcal{N}_y$. If the mesh is uniformly spaced in each axis direction, $(x_{\ell+1} - x_\ell) = (x_{\ell+2} - x_{\ell+1})$, $\ell = 1, \ldots, \mathcal{N}_x - 2$ and $(y_{\ell+1} - y_\ell) = (y_{\ell+2} - y_{\ell+1})$, $\ell = 1, \ldots, \mathcal{N}_y - 2$. Permittivities are considered constant within each mesh element (for simplicity only) and are denoted $\epsilon_{k\ell}$, $k = 1, \ldots, \mathcal{N}_x - 1$ and $\ell = 1, \ldots, \mathcal{N}_y - 1$. Define centered finite-differences of the potential ψ in the x- and y-axis directions at the midpoints of element edges as follows:

$$\Delta^x_{k+\frac{1}{2},\ell} \doteq -\frac{\psi_{k+1,\ell}-\psi_{k\ell}}{x_{k+1}-x_k}\,, \qquad \Delta^y_{k,\ell+\frac{1}{2}} \doteq -\frac{\psi_{k,\ell+1}-\psi_{k\ell}}{y_{\ell+1}-y_\ell}\,, \tag{2}$$

where the minus sign is included for convenience because electric field is the negative of the gradient of potential. Here, the superscript denotes the direction of the difference and the subscript locates the midpoint of the element edge where the difference is second-order accurate. Where two indices are used to refer to a mesh node, the indices are written (i, j), while two indices written $\langle i, j\rangle$ refer to the mesh element defined by the nodes (i, j), $(i+1, j)$, $(i, j+1)$ and $(i+1, j+1)$. Fig. 1 shows a portion of a two-dimensional tensor-product mesh illustrating the notation for meshlines and permittivities. The differences defined in Eq. (2) would, for example, be located at the positions of the open dots in Fig. 1.

Consider a point charge in 2D (*i.e.*, a line charge) ρ_L located at (x, y) within an element $\langle i, j\rangle$ (*i.e.*, the central element in Fig. 1). If restrictions (P) and (M) apply, the standard NGP/CIC schemes in two dimensions can be summarized by the following four steps:

1. *charge assignment to the mesh*: The portion of ρ_L assigned to the element nodes (k, ℓ) are $w_{k\ell}\rho_L$, $k = i, i+1$ and $\ell = j, j+1$, where $w_{k\ell}$ are the four charge weights which sum to unity by charge conservation. For the NGP scheme, the node closest to (x, y) receives a weight $w_{k\ell} = 1$, with the remaining three weights set to zero. For the CIC scheme, the weights are $w_{ij} = w_x w_y$, $w_{i+1,j} = (1 - w_x)w_y$, $w_{i,j+1} = w_x(1 - w_y)$ and $w_{i+1,j+1} = (1 - w_x)(1 - w_y)$, where $w_x = (x_{i+1} - x)/(x_{i+1} - x_i)$ and $w_y = (y_{j+1} - y)/(y_{j+1} - y_j)$.

2. *solve the Poisson equation*: The Poisson equation $-\nabla \cdot (\epsilon\nabla\psi) = \rho$ is solved by some appropriate numerical technique for the potential ψ defined at the mesh nodes. Here ρ contains contributions from both mobile charges, doping and fixed charges, as appropriate.

3. *compute forces on the mesh*: The electric field at mesh nodes (k, ℓ), $\vec{E}_{k\ell} = [E^x_{k\ell};\ E^y_{k\ell}]$, is computed as $E^x_{k\ell} = (\Delta^x_{k-\frac{1}{2},\ell} + \Delta^x_{k+\frac{1}{2},\ell})/2$ and $E^y_{k\ell} = (\Delta^y_{k,\ell-\frac{1}{2}} + \Delta^y_{k,\ell+\frac{1}{2}})/2$, for $k = i, i+1$ and $\ell = j, j+1$.

4. *interpolate to find force on the charge*: Interpolate the field to position (x, y), $\vec{E}(x, y) =$

$[E^x;\, E^y]$, according to $E^x = \sum_{k,\ell} w_{k\ell} E^x_{k\ell}$ and $E^y = \sum_{k,\ell} w_{k\ell} E^y_{k\ell}$, where $k = i, i+1$, $\ell = j, j+1$ and the w_{ij} are the NGP or CIC weights from step 1.

An improved NGP/CIC scheme can be obtained by altering only step 3 above. These schemes (denoted NGP* and CIC*) are appropriate for the case when permittivity depends on position, yet the mesh spacing is still uniform in each axis direction (*i.e.*, restriction (P) removed and (M) still holds). For the NGP* and CIC* schemes, the new step 3 becomes:

3*. *compute forces on the mesh*: Calculate the mesh-defined electric field at the four nodes (k,ℓ), $\vec{E}_{k\ell} = [E^x_{k\ell};\, E^y_{k\ell}]$, as $E^x_{k\ell} = (\epsilon_{k-1,j}\, \Delta^x_{k-\frac{1}{2},\ell} + \epsilon_{kj}\, \Delta^x_{k+\frac{1}{2},\ell})/(2\epsilon_{ij})$ and $E^y_{k\ell} = (\epsilon_{i,\ell-1}\, \Delta^y_{k,\ell-\frac{1}{2}} + \epsilon_{i\ell}\, \Delta^y_{k,\ell+\frac{1}{2}})/(2\epsilon_{ij})$, for $k = i, i+1$ and $\ell = j, j+1$.

To understand the improvement so obtained, consider a one-dimensional model problem. A discussion of the performance of these and other PM schemes in two dimensions is deferred to the next section.

Consider a silicon MOS capacitor-like problem: undoped Si extends for $0 \le x \le 35$ nm and SiO_2 covers $35 < x \le 50$ nm. A substrate contact at $x = 0$ nm is grounded; a gate contact at $x = 50$ nm is set to 1 V (the work function for the contact to the insulator is chosen to yield a flat-band voltage of 0 V). A single point charge in 1D (*i.e.*, a plane of charge) $\rho_A = -2 \times 10^{12}\,\mathrm{cm}^{-2}$ is placed at *any* position within the model. The force acting upon the charge is computed as a function of the charge's position within the "device", and is show in Fig. 2. This figure actually shows five such plots, each vertically displaced from the other as indicated by the dotted baselines corresponding to a zero force value. The upper-most curve, marked CIC, gives the result for the standard CIC scheme. The next curve down, marked CIC*, shows the result for the improved CIC scheme. The bottom curve, marked "EXACT", gives the exact solution for this model problem. (Curves marked NEC and NEC–CIC* to be discussed shortly.) The CIC* scheme is seen to greatly improve the resolution of the force near the Si-SiO_2 interface located at 35 nm, compared to the standard CIC scheme. This is the hallmark of the "$\star$" schemes: better force resolution near regions of differing permittivity. Note, however, that both CIC and CIC* do a poor job of force resolution near the two contacts (x = 0 and x = 50 nm) compared to the exact solution. To address this problem, the NEC scheme is proposed.

The NEC charge assignment/force interpolation scheme attempts to reduce self forces and increase spatial accuracy in the presence of non-uniformly spaced tensor-product meshes and/or spatially-dependent permittivity, *i.e.*, restriction (P) is removed and (M) is relaxed. In addition, the NEC scheme can be utilized in one axis direction (where local mesh spacing is non-uniform) and the CIC* scheme can be utilized in the other (where local mesh spacing is uniform). Such hybrid schemes, dubbed NEC-x–CIC*-y or NEC-y–CIC*-x, offer smoother assignment/interpolation on the mesh compared to pure NEC. These schemes will be described for a two-dimensional mesh.

Consider a line charge ρ_L residing at (x, y) in a rectangular mesh element $\langle i, j\rangle$ with permittivity ϵ_{ij}. The new steps of the (pure-)NEC PM scheme are:

1$'$. *charge assignment to the mesh*: Divide the line charge ρ_L *equally* to the four mesh points of the element $\langle i, j\rangle$;

3$'$. *compute forces on the mesh*: Calculate the fields $\Delta^x_{i+\frac{1}{2},\ell}$, $\ell = j, j+1$, and $\Delta^y_{k,j+\frac{1}{2}}$, $k = i, i+1$;

4$'$. *interpolate to find force on the charge*: Interpolate the field $\vec{E}(x, y) = [E^x;\ E^y]$, according to $E^x = (\Delta^x_{i+\frac{1}{2},j} + \Delta^x_{i+\frac{1}{2},j+1})/2$, $E^y = (\Delta^y_{i,j+\frac{1}{2}} + \Delta^y_{i+1,j+\frac{1}{2}})/2$.

The NEC designation derives from the appearance, in step 1$'$, of moving the charge to the center of its element and applying a CIC-like assignment scheme. The NEC scheme involves *only* one mesh element and its four nodal values of potential. This locality makes the method well-suited to non-uniform mesh spacings and permittivity.

The NEC-x–CIC*-y scheme is designed to involve only $\langle i, j\rangle$ elemental quantities for x-directed fields, but not for y-directed fields. The new steps of the NEC-x–CIC*-y scheme are:

1$''$. *charge assignment to the mesh*: Conceptually move the charge from its location (x, y) to $(\bar{x}, y)$, where $\bar{x} = 0.5(x_i + x_{i+1})$, and apply the CIC charge weighting scheme (denote these CIC weights as w_{ij}, $w_{i+1,j}$, $w_{i,j+1}$ and $w_{i+1,j+1}$; note $w_{ij} = w_{i+1,j}$ and $w_{i,j+1} = w_{i+1,j+1}$ in this case);

$3''$. *compute forces on the mesh*: Calculate fields $\Delta^x_{i+\frac{1}{2},j}$ and $\Delta^x_{i+\frac{1}{2},j+1}$ as in pure-NEC; calculate fields $E^y_{k\ell}$, $k = i, i+1$ and $\ell = j, j+1$ as in CIC*;

$4''$. *interpolate to find force on the charge*: Interpolate the field $\vec{E}(x,y) = [E^x;\, E^y]$ according to $E^x = (w_{ij} + w_{i+1,j})\Delta^x_{i+\frac{1}{2},j} + (w_{i,j+1} + w_{i+1,j+1})\Delta^x_{i+\frac{1}{2},j+1}$, $E^y = \sum_{k,\ell} w_{k\ell} E^y_{k\ell}$ for $k = i, i+1$ and $\ell = j, j+1$, where the w_{ij} are the CIC weights from step $1''$.

The other mixed scheme, NEC-y–CIC*-x, is defined analogously.

The mixed schemes provide for smoother assignment and interpolation in the "CIC" direction compared to the application of a pure-NEC scheme. In a device simulation context, the decision whether to apply NEC or CIC* in a given direction (the x-axis direction, for example) in the vicinity of element $\langle i,j\rangle$ is: *if* the local x-axis mesh spacing is constant (*i.e.*, $x_i - x_{i-1} = x_{i+1} - x_i = x_{i+2} - x_{i+1}$) *and* none of the nodes (k,ℓ), $k = i, i+1$ and $\ell = j, j+1$ are contact nodes, *then* CIC* should be used; *otherwise*, NEC should be employed. Applying analogous rules in the y-axis direction leads to four outcomes for element $\langle i,j\rangle$: pure NEC or CIC*, or the two hybrid schemes.

Returning to the one-dimensional model problem and Fig. 2, the pure-NEC scheme yields the force versus charge position curve marked NEC. The decrease in smoothness is evident, as the force is approximated as "steps". Note, however, the behavior near the two contacts (x = 0 and x = 50 nm) is superior to both CIC and CIC* schemes. Applying a mixed scheme obtains the best overall approximation to the exact force solution, as seen by the curve marked NEC–CIC*. Because the mesh is uniform in Fig. 2, the NEC–CIC* scheme equals the CIC* scheme everywhere except near contacts. Near the two contacts the NEC–CIC* scheme adopts the NEC behavior as stipulated by the discussion of the previous paragraph.

Fig. 3 revisits this same one-dimensional model problem, except for one change: the various PM schemes are now exercised on a nonuniform mesh. The mesh is uniform away from the Si-SiO_2 interface with a graded refinement as the interface is approached. The features to note in Fig. 3 are as follows. First, both CIC and CIC* schemes behave poorly near the semiconductor–insulator interface: the CIC scheme because of the nonuniform mesh *and* the change in permittivity (the former dominating), the CIC* because of the nonuniform mesh. The inadvisability of applying CIC or CIC* schemes to nonuniform meshes is clear, as the force is overestimated and nonmonotonic near the interface. Behavior near the two contacts remains poor as in the uniform mesh case. Secondly, the NEC scheme does an admirable job of obtaining the force throughout the model in a piecewise-constant approximation. Finally, the mixed scheme (marked NEC–CIC*) adopts linear force behavior in region of local mesh uniformity and a piecewise-constant approximation otherwise and is again the best representation of the exact solution.

The NEC scheme, and the two mixed schemes, described in this section do not maintain zero self force exactly. Rather, self force is expected to be small to the extent that the well behaved forces (WBF) assumption is obeyed for a given mesh. Appendix A explains the WBF assumption and verifies computationally that it is an excellent assumption in practice. Appendix B derives the self force for the PM schemes discussed in this paper, showing each to be properly formulated to reduce or eliminate self force. Appendix C describes how the new PM schemes fit into a hierarchy of schemes as defined in Ref. [1].

4 CIC* and NEC Schemes in Two Dimensions

In Sec. 3 the superiority of the mixed scheme NEC–CIC* compared to CIC, CIC* or NEC was demonstrated for a one-dimensional model problem. In this section, a two-dimensional model problem is defined and the performance of the PM schemes investigated. The outcome of this investigation is not a forgone conclusion, for one reason: the potential singularity in one dimension for a plane charge is a piecewise linear, continuous function; in two dimensions, it is a logarithmic function of distance from the line charge. The latter form is far less amenable to a finite difference representation truncated to second order. This is an issue of spatial accuracy, which permeates the subsequent discussion.

4.1 A Two-Dimensional Model Problem

The two-dimensional model problem consists of a square domain $0 \leq x \leq 100$ nm and $0 \leq y \leq 100$ nm. In the region $0 \leq y \leq 50$ nm the model consists of n-type Si uniformly doped 10^{18} cm^{-3}; for $50 < y \leq 100$ nm the model consists of SiO_2. The entire perimeter (semiconductor *and* insulator) is a single Dirichlet boundary set to 0 V (the work function for the contact to the insulator is chosen to yield a flat-band voltage of 0 V). A line charge of value ρ_L is placed at location (x, y) anywhere within the model, and the x- and y-directed force on this single line charge is determined. To facilitate comparisons between the various PM schemes, two paths through the domain are defined; force is plotted as a function of position as the charge is moved along these paths. Path 1 consists of a straight line segment from $(400, 0)$ to $(600, 1000)$ nm; this path moves from Si to SiO_2 at its midpoint and cuts the Si-SiO_2 interface at an angle of $\sim 79°$. Path 2 consists of a straight line segment from $(0, 400)$ to $(1000, 600)$ nm; this path also moves from Si to SiO_2 at its midpoint and cuts the Si-SiO_2 interface at an angle of $\sim 11°$. Two different 25×25 node meshes are used in these computations: a uniformly-spaced mesh ($\Delta x = \Delta y = 4.17$ nm) and a nonuniformly-spaced mesh (x-mesh intervals consist of 7 equal intervals, followed by 5 intervals of decreasing length by a factor $0.9\times$, followed by 5 intervals of increasing length by a factor $1.11\times$, and ending with 7 equal intervals; y-mesh intervals same as x-mesh intervals).

The value ρ_L of the line charge is not arbitrarily chosen; rather, in Ref. [6] it is argued that the linear charge density $\rho_L = \mathcal{S} \lesssim \Delta x^{-1}$, where Δx is the mesh spacing, so that density fluctuations in two dimensions have amplitudes representative of real density fluctuations in three dimensions. A more careful argument[7] related to screening shows $\rho_L \leq \frac{1}{2\Delta x}$ is a better upper bound on the linear charge density ρ_L. Since the mesh size used for the computations has $\Delta x \sim 4.2$ nm, and desiring a negative charge density, this yields a maximum $\rho_L = -1.2 \times 10^6$ cm^{-1}.

Fig. 4 shows the x-directed force acting on the line charge as it traverses path 1, with position along the path indicated by the y-coordinate value of the charge. The force is sinusoidal in appearance, but asymmetric because of the two regions of differing permittivity. Four PM schemes are contrasted: standard and improved CIC (marked CIC and CIC*), NEC and the combination of CIC*, NEC-y–CIC*-x, NEC-y–CIC*-x and NEC (marked NEC–CIC*, and combined according to the rule discussed in Sec. 3). A numerical approximation to the exact solution computed on a much finer mesh (marked EXACT) is shown for comparison. The CIC and CIC* results (equal because the force direction runs parallel to the Si-SiO_2 interface) are impressive in their accuracy. The NEC result is a piecewise constant approximation, with the added feature that major "steps" occur when the path crosses an x-meshline and smaller "steps" when the path crosses an y-meshline. Since the NEC scheme conceptually moves the charge to the element center, these steps are a signature of the discrete manner in which the charge "moves" from center to center of the elements which intersect path 1. The mixed method NEC–CIC* is identical to CIC and CIC* results except at the ends of the path ($y = 0$ and 100 nm) since the present of a contact triggers a switch over to NEC behavior. Except for this behavior at the contacts, the mixed method again represents the PM scheme of choice. This behavior near the contacts is necessary, once the y-directed force acting on the charge is examined.

Fig. 5 is similar to Fig. 4 except that the y-directed force acting on the charge is shown. Note the ordinate scale factor indicates y-directed forces are much larger than the x-directed forces shown in Fig. 4; this is anticipated for path 1 since it straddles the symmetry line $x = 50$ nm for the model problem along which the x-directed force will be identically zero. The structure of the exact solution deserves comment, before the results for the four PM schemes are examined. This exact solution contains singularities near the contacts and at the Si-SiO_2 interface. Both behaviors are anticipated. As the line charge approaches a contact, charge of the opposite sign is induced on the contact, causing an attractive force. This force is directed so as to push the charge towards the contact and is unbounded as the distance approaches zero. As the line charge approaches the Si-SiO_2 interface, an image force conceptually resides on the opposite side of the interface. This image force will differ in polarity if the permittivity on the opposite side of the interface is greater than the permittivity of the side where the line charge resides[8]. Thus, while on the Si side, the charge is repulsed by the interface, and while on the SiO_2 side, the charge is attracted to the interface. In both cases, a negative and unbounded force results as the interface is approached. The presence of singularities in the exact solution present a difficulty not seen in the one-dimensional model problem. Nevertheless, the results for the four PM schemes shown in Fig. 5 follows the trends obtained from the one-dimensional model problem. The CIC scheme fails near the Si-SiO_2 interface ($y = 50$ nm) and near the contacts ($y = 0$ and 100 nm); in the former case, the force is underestimated and poorly resolved, while in the latter case, the force is of the wrong polarity. The CIC* results in excellent (but bounded) behavior near the Si-SiO_2 but remains in error at the contacts. The NEC scheme is globally accurate, but less smooth due to the piecewise constant nature of the force approximation. The NEC–CIC* scheme essentially captures the best behaviors of the separate NEC and CIC* schemes: near the contacts, NEC-like behavior prevails and near the interface, CIC*-like behavior prevails. Within the constraints of the mesh spacing used, and the fact that computed force remains finite for finite mesh refinement, NEC–CIC* does an acceptable job of resolving the singularities in the y-directed force.

The next two figures present the results of the same computation, sampling the results on path 2. Along this path, which straddles the Si-SiO_2 interface, the x-directed force is of a similar magnitude as the y-directed force. Fig. 6 shows the x-directed force for the four PM schemes, as well as an approximation to the exact solution computed on a much finer mesh. Singularities in the force are observed at the contacts at $x = 0$ and 100 nm, in a polarity to push the charge towards the contact. The CIC and CIC* schemes are extremely accurate, except in resolving these singularities. The NEC scheme is essentially a staircase approximation to these results. The NEC–CIC* scheme reproduces CIC* behavior away from the contacts, and NEC behavior near the contacts. Again, the need to switch over to NEC at the contacts is not motivated by the x-directed force, but rather, the y-directed force as shown in Fig. 7.

Fig. 7 shows the y-directed force along path 2. The exact solution contains the anticipated singularity at the Si-SiO_2 interface (when $x = 50$ nm), but correctly approaches zero near the contacts at $x = 0$ and 100 nm. The CIC results are very poor with regards to resolving behavior near the interface. For x-coordinates values $29.2 \leq x \leq 70.8$ nm, the line charge resides within mesh elements which border on the Si-SiO_2 interface. For these elements, CIC does not take the proximity to a change in permittivity into account, and results in a very poor force resolution. CIC* does an acceptable job of obtaining the force except for two artifacts: the inability to resolve the force singularity at the interface, and the scalloped appearance of the force (with increasing amplitude as the interface is approached). The former artifact is ameliorated by increasing the mesh resolution; only five mesh lines parallel to the interface are traversed by path 2. The latter artifact is intrinsic to the CIC* scheme. Because this behavior is unwelcome, it is discussed at length in Sec. 4.2.

The behavior of the four schemes when applied to the model problem posed on a nonuniform mesh can be readily summarized. Mesh nonuniformity is not handled properly by the CIC and CIC* schemes; as a result, in regions of local mesh nonuniformity these methods generally result in a poor force computation. The NEC scheme was designed for just such local mesh nonuniformity; within the limits of a piecewise constant approximation, the forces computed are quite reasonable. The NEC–CIC* scheme reverts to NEC behavior in regions of local mesh nonuniformity and thus remains the method of choice of the four PM methods. Fig. 8 reports the magnitude of the force on the line charge as it traverses path 2, and shows results consist with this summary. Note the NEC–CIC* does not show a scalloped force characteristic near the interface because the mesh nonuniformity there caused the scheme to adopt NEC behavior.

While many other combinations have been examined, the previous remarks serve to capture the essential character of the four PM methods in two-dimensions. But what causes the scalloped force versus position curves seen in Figs. 7 and 8?

4.2 Cause of the "Scallops" in the Force

Figs. 7 and 8 show unwelcome scalloping in some of their force versus position results. In Fig. 7, they are obvious in CIC* and NEC–CIC* results, but also present in the CIC curve. In Fig. 8, their presence in the y-directed force for the CIC and CIC* schemes causes them to appear in the corresponding curves for the magnitude of the force. The imperfect attempt to resolve the force between line charge and its image charge in the vicinity of and normal to the Si-SiO$_2$ interface is the cause of this scalloping.

Fig. 9 shows a contour plot of the y-directed force for the two-dimensional model problem posed on a uniform mesh, computed with the CIC* scheme. Only a small subregion of the entire mesh (16 elements out of 576) is shown. This subregion lies entirely in SiO$_2$; the lower-left corner point $(50, 50)$ nm is the center of the model problem. The lower edge of the subregion sits along the Si-SiO$_2$ interface. The location of the two paths as they traverse the subregion are indicated. The portion of path 1 shown corresponds to the CIC* results shown in Fig. 5 with $50 \leq y \leq 66.67$ nm. There is no scalloping, but referring to Fig. 9 indicates path 1 samples the y-directed force along a path sufficiently perpendicular to the Si-SiO$_2$ and fortuitously avoids nonmonotonic behavior. The portion of path 2 shown corresponds to the CIC* results shown in Fig. 7 with $50 \leq y \leq 66.67$ nm. Here the path cuts the force results in such a way as to obtain a scalloped appearance. In Fig. 9 it is clear that the y-directed force is larger at the interface when the charge resides upon x-meshlines, and is less when the charge resides midway between x-meshlines. To explain this behavior, consider first the analytic behavior of the potential near the Si-SiO$_2$ interface, for it is the potential which is differenced to obtain the force.

Consider a line charge ρ_L in the 2D Cartesian plane located at $(0, d)$, a distance $d > 0$ from a dielectric boundary $y = 0$ in an otherwise infinite domain. If the permittivity is ϵ_1 for $y > 0$ and ϵ_2 for $y < 0$, then the potential is[8]

$$V(x,y) = -\frac{\rho_L}{2\pi\epsilon_1} \ln\sqrt{x^2 + (y-d)^2} - \frac{\rho_L}{2\pi\epsilon_1}\left(\frac{\epsilon_1 - \epsilon_2}{\epsilon_1 + \epsilon_2}\right) \ln\sqrt{x^2 + (y+d)^2}\,, \quad y > 0\,. \tag{3}$$

The scalloping in the y-directed force can now be estimated. Consider a line charge within the subregion of Fig. 9. Assuming the charge is far enough from the boundaries of the model problem, and neglecting the force due to the presence of the doping, the computed potential can be estimated with the help of Eq. (3). Define the potential difference at position (s, d) as

$$\mathcal{D}(s,d) = \lim_{\lambda \to 0} \frac{V(s, d+\lambda) - V(s, d-\lambda)}{2\lambda} = -\frac{\rho_L}{2\pi\epsilon_1}\left(\frac{\epsilon_1 - \epsilon_2}{\epsilon_1 + \epsilon_2}\right) \frac{2d}{s^2 + (2d)^2}\,. \tag{4}$$

For simplicity, consider how the y-directed force from the CIC* scheme varies as the charge is moved parallel to the interface along a y-meshline. First, consider ρ_L located at the node (i, j). The force on the charge will be equal to the force computed at this node, the magnitude of which is readily estimated as $\mathcal{D}(0, d)$. Now move ρ_L one-half mesh spacing away this node along the y-meshline, *i.e.*, to $(i + \frac{1}{2}, j)$. The charge resides midway between two nodes; the force is the average of the forces at nodes (i, j) and $(i + 1, j)$, where each node has a charge of $\frac{1}{2}\rho_L$. The force is estimated from a superposition of the potential solutions for the two charges. The charge at node (i, j) contributes a force $\frac{1}{2}\mathcal{D}(0, d)$ to node (i, j) and $\frac{1}{2}\mathcal{D}(\Delta x, d)$ to node $(i + 1, j)$, where $\Delta x = x_{i+1} - x_i$. The charge at node $(i + 1, j)$ contributes a force $\frac{1}{2}\mathcal{D}(0, d)$ to node $(i + 1, j)$ and $\frac{1}{2}\mathcal{D}(-\Delta x, d) = \frac{1}{2}\mathcal{D}(\Delta x, d)$ to node (i, j). Thus, the force at both nodes (i, j) and $(i + 1, j)$ is $\frac{1}{2}\left[\mathcal{D}(0, d) + \mathcal{D}(\Delta x, d)\right]$; the average of these equal values gives the estimate of the force for the original line charge located at $(i + \frac{1}{2}, j)$. Thus, on x-meshlines, the force estimate is $\mathcal{D}(0, d)$, while midway between x-

meshlines, the force estimate is $\frac{1}{2}\left[\mathcal{D}(0,d)+\mathcal{D}(\Delta x,d)\right]$. The ratio of the former to the latter quantifies the magnitude of the scalloping in the y-directed force; this ratio $\mathcal{R}(\Delta x,d)$ is

$$\mathcal{R}(\Delta x,d)=\frac{\mathcal{D}(0,d)}{\frac{1}{2}\left[\mathcal{D}(0,d)+\mathcal{D}(\Delta x,d)\right]}=\frac{2+8\left(\frac{d}{\Delta x}\right)^2}{1+8\left(\frac{d}{\Delta x}\right)^2}\quad . \tag{5}$$

This estimate is consistent with the observed behavior (the scalloping in Figs. 7 and 8 is less on the Si side than the SiO_2 side due to presence of the doping). The scalloping behavior, as revealed by the estimate in Eq. (5), is independent of permittivities and linear charge density. It depends only on the ratio of the distance of the charge from the interface to the mesh spacing parallel to the interface. The scalloping is worst at the interface ($d=0$), where the ratio $\mathcal{R}=2$. However, this ratio approaches unity quadratically as the charge moves away from the interface; for example, when $d=\Delta x$, *i.e.*, the charge is as far from the interface as the mesh spacing parallel to the interface, $\mathcal{R}=\frac{10}{9}$.

In spite of this unwelcome scalloping behavior in the force perpendicular to the Si-SiO_2 interface, its effect is local to the interface and estimated to be bounded in magnitude. This is considered acceptable, especially compared to making no attempt to incorporate the force due to the image force present at a change in permittivity; therefore, a mixed NEC–CIC* scheme remains the PM scheme of choice for general semiconductor problems. Nevertheless, improvements which reduce the scalloping would be welcomed.

5 What About Unstructured Triangular Meshes?

The NEC PM scheme and its combinations NEC-x–CIC*-y and NEC-y–CIC*-x are applicable to problems with spatially-dependent permittivity on nonuniformly-spaced tensor-product meshes, *i.e.*, restriction (P) is removed and restriction (M) is relaxed. It is natural to ask: can restriction (M) be removed and unstructured meshes of triangular elements be used instead? Both good spatial accuracy and small self force are desired. Particle-mesh coupling on triangular meshes have been utilized in other disciplines using 2D unstructured triangular meshes[9], 2D structured triangular meshes[10] and 3D unstructured tetrahedral meshes[11]. It seems reasonable to seek a PM scheme which only involves a single triangular mesh element, as this should be compatible with the goal of using an unstructured triangular mesh. The simplest such scheme could use a to-be-determined charge assignment and a piecewise linear potential within the triangular element (linear shape functions on triangular elements[12]). The scheme considered here resembles that of Ref. [9], but with a simplified force interpolation step.

Following the procedure described in Appendix B, the charge assignment scheme which reduces self force is sought. Consider a triangular element $\mathcal{T}$ with nodes i, j, k in an unstructured triangular mesh of infinite spatial extent. A line charge ρ_L resides at (x, y) within $\mathcal{T}$. Assume the potential is a linear function of position within $\mathcal{T}$, *i.e.*, $\psi(x,y) = \psi_i N_i(x,y) + \psi_j N_j(x,y) + \psi_k N_k(x,y)$, where the $N_\ell(x,y)$ are the linear shape functions associated with $\mathcal{T}$[12]. The four steps of the proposed PM scheme are:

$1^\triangle$. *charge assignment to the mesh*: Charge assignment is left unspecified; assign charge to nodes as $\varrho \doteq [\rho_i\, \rho_j\, \rho_k]^T = \rho[c_i\, c_j\, c_k]^T \doteq \rho\mathbf{c}$, where $\sum_{\ell=i,j,k} c_\ell = 1$ by charge conservation.

$2^\triangle$. *solve the Poisson equation*: Solve the Poisson equation; the charges at the nodes will result in a potential $\varphi = \mathbf{G}\varrho$, where $\varphi = [\psi_i\, \psi_j\, \psi_k]^T$ and $\mathbf{G} = (g_{ij})$ is a 3×3 matrix extracted from the rows and columns $\{i, j, k\}$ of the inverse of the Laplacian on the infinite mesh. The WBF assumption dictates the form of $\mathbf{G}$: diagonal entries are all equal and the matrix is symmetric. Therefore,

$$\mathbf{G} = \begin{pmatrix} g_{ii} & g_{ij} & g_{ik} \\ g_{ji} & g_{jj} & g_{jk} \\ g_{ki} & g_{kj} & g_{kk} \end{pmatrix} \overset{\substack{\text{from}\\ \text{WBF}}}{=} \begin{pmatrix} g_{ii} & g_{ij} & g_{ik} \\ g_{ij} & g_{ii} & g_{jk} \\ g_{ik} & g_{jk} & g_{ii} \end{pmatrix} = g_{ii} \begin{pmatrix} 1 & \alpha & \beta \\ \alpha & 1 & \gamma \\ \beta & \gamma & 1 \end{pmatrix} \doteq g_{ii}\tilde{\mathbf{G}}, \quad (6)$$

where $0 < \alpha, \beta, \gamma < 1$, $\alpha \neq \beta \neq \gamma$ in general and the WBF assumption is applied in triangle $\mathcal{T}$ (cf. Appendix A).

$3^\triangle$–$4^\triangle$. *compute forces on the mesh/interpolate to find force on the charge*: The electric field in $\mathcal{T}$ is the constant vector $\vec{E} = -\nabla\psi = -\sum \psi_\ell \nabla N_\ell$. Since the field in $\mathcal{T}$ is everywhere the same, field interpolation is automatically accomplished.

A *zero* field on the original line charge ρ_L is sought; therefore, the field in step $4^\triangle$ should be zero. Obtaining $\vec{E} = \vec{0}$ occurs only if $\psi_i = \psi_j = \psi_k$. A charge weighting scheme $\mathbf{c}$ that gives equal nodal potentials obeys:

$$\mathbf{G}\varrho = g_{ii}\rho\tilde{\mathbf{G}}\mathbf{c} = \varphi \propto [1\,1\,1]^T \rightarrow\ \tilde{\mathbf{G}}\mathbf{c} \propto [1\,1\,1]^T . \quad (7)$$

This has a complicated solution ($\mathbf{c} \propto \tilde{\mathbf{G}}^{-1}[1\,1\,1]^T$) and a simple solution ($c_i = c_j = c_k = \frac{1}{3}$, if $\alpha = \beta = \gamma$). To be useful, the charge weights $\mathbf{c}$ should be local functions of the element $\mathcal{T}$ (cf. Appendix B); since α, β and γ are global functions of the entire mesh, $\mathbf{c}$ should be independent of α, β and γ. This requires the complicated solution be discarded. The simple solution obtains $\mathbf{c}$ independent of α, β and γ as required, but only when $\alpha = \beta = \gamma$. This implies the mesh be composed of identically-sized equilateral triangles, which is not a very useful "unstructured" triangular mesh! Can a useful PM coupling for unstructured triangular meshes be designed which yields zero self forces (in the WBF sense)? To my knowledge this important question remains unanswered.

6 Conclusions

The NEC*, CIC* and NEC PM schemes are proposed to reduce self forces. Hybrid combinations of these methods are described. An attempt to design a PM scheme for unstructured triangular meshes is successful only for meshes of equilateral triangles.

7 Acknowledgment

Countless discussions with M.V. Fischetti are gratefully acknowledged. D.J. Frank contributed many useful suggestions to the early stages of this work. J.M. Higman is thanked for pointing out Ref. [10]. This manuscript has been read in draft form by M.V. Fischetti.

Appendix A The WBF Assumption

The well behaved forces (WBF) assumption is used in conjunction with inquires into self forces of various PM schemes; to this end, and to be specific to the two-dimensional case, consider a single line charge ρ_L located on a two-dimensional mesh of infinite spatial extent, constant permittivity and no boundaries. The WBF assumption considers the potential computed due to a single charge depends only on the magnitude of the distance from the charge to the point in question, independent of the underlying (infinite) mesh structure. The continuum solution of the Poisson equation in this case has this form, as the solution to $-\nabla \cdot (\epsilon \nabla \psi) = \rho_L \, \delta(x - x_0) \, \delta(y - y_0)$ is

$$\psi(x, y) = -\frac{\rho_L}{2\pi\epsilon} \ln(r) + \text{const.} \,, \tag{8}$$

where $r = \sqrt{(x - x_0)^2 + (y - y_0)^2}$. Since the force is proportional to the gradient of the potential ψ, this form of the potential also implies force due to a single charge depends only the magnitude and direction of the distance from the charge to the point in question. Since the continuum solution to the Poisson equation obeys the assumption, and since the discrete case seeks to solve the same Poisson equation, the WBF assumption seems like a reasonable assertion.

This assumption can be proven rigorous in the case where the mesh is a tensor-product mesh with constant mesh spacing in each of the x- and y-axis directions, and is used by Hockney and Eastwood to demonstrate that NGP and CIC schemes guarantee zero self force[1]. How good is this assumption for tensor-product meshes with nonuniform mesh spacing?

Computations were performed to examine the error in the WBF assumption for five different tensor-product meshes. Such a computation should solve the Poisson equation on a mesh of infinite size with boundary conditions imposed only infinitely far from a single line charge ρ_L. The actual computation is done on a square mesh of finite extent; the influence of finite size and boundaries will be examined below. The Poisson equation was solved on a 100×100 mesh covering the unit square in the two-dimensional Cartesian plane. The perimeter of the square assumed zero-normal derivative boundary conditions for the potential, except for the node at the origin, which was set to a fixed potential of zero. Label the mesh element which is as far from the perimeter of the unit square as possible as element $\mathcal{E}$, and for convenience, index the four nodes of $\mathcal{E}$ by 1,2,3,4. The following computations were performed: a single line charge is place at node 1, the Poisson equation is solved, and the potential is obtained at all four nodes. These four potential values are divided by the line charge value ρ_L and are placed in the first column in a 4×4 matrix $\mathbf{G}$. This process is repeated for the charge being located at node 2, 3 and 4, being stored into the second, third and fourth columns of $\mathbf{G}$, respectively. The matrix $\mathbf{G}$ quantifies the coupling between charge and resultant potential at the four nodes, according to

$$\varphi = \begin{bmatrix} \psi_1 \\ \psi_2 \\ \psi_3 \\ \psi_4 \end{bmatrix} = \mathbf{G}\varrho = \begin{pmatrix} g_{11} & g_{12} & g_{13} & g_{14} \\ g_{21} & g_{22} & g_{23} & g_{24} \\ g_{31} & g_{32} & g_{33} & g_{34} \\ g_{41} & g_{42} & g_{43} & g_{44} \end{pmatrix} \begin{bmatrix} \rho_{L1} \\ \rho_{L2} \\ \rho_{L3} \\ \rho_{L4} \end{bmatrix} \underset{\text{WBF}}{\overset{\text{from}}{=}}$$

$$g_{11} \begin{pmatrix} 1 & \alpha & \beta & \gamma \\ \alpha & 1 & \gamma & \beta \\ \beta & \gamma & 1 & \alpha \\ \gamma & \beta & \alpha & 1 \end{pmatrix} \begin{bmatrix} \rho_{L1} \\ \rho_{L2} \\ \rho_{L3} \\ \rho_{L4} \end{bmatrix} = g_{11}\tilde{\mathbf{G}}\varrho \ , \tag{9}$$

where ψ_ℓ and $\rho_{L\ell}$ are the values of the potential and the line charge density at the node ℓ, $\ell = 1, \ldots, 4$. If the computation approximates the infinite mesh behavior near element $\mathcal{E}$, then the $\mathbf{G}$ computed should conform to the form dictated by the WBF assumption as shown in Eq. (9). If the mesh were infinite in extent, the WBF assumption would dictate the form of $\mathbf{G}$ from three observations: (*i*) $\mathbf{G}$ must be symmetric, because potential depends only on the distance between the charge and a given location; (*ii*) all diagonal entries must be equal, because potentials at charge locations are equal (note the potential will *not* be infinite in the discrete case); and (*iii*) there are only three unique off-diagonal entries, because there are only three relevant distances in the rectangular element $\mathcal{E}$ (the lengths of the sides of the rectangular element, and the length of the diagonal of the rectangular element).

The first 100×100 mesh examined (mesh A) has uniform (and equal) mesh spacing in x- and y-axis direction (the element $\mathcal{E}$ is 0.0101×0.0101 in size). This is really a sanity check to insure the finite mesh size and presence of boundary condition does not damage the $\mathbf{G}$ computed, for a proof of the validity of the WBF assumption exists for such a mesh[1]. The results are exactly as expected, to a very high degree of accuracy, as seen in Table 1, with values that differ by less than 0.2% from the WBF form.

Four nonuniform meshes were then considered. Mesh B is uniform in the y-axis direction; the x-axis consists of 32 intervals of length 0.0155 followed by 67 intervals of length 0.0075 (the element $\mathcal{E}$ is 0.0075×0.0101 in size). Mesh C is uniform in the y-axis direction; the x-axis consists of 33 intervals of length 0.0154 followed by 66 intervals of length 0.0075 (the element $\mathcal{E}$ is 0.0154×0.0101 in size). Mesh D is uniform in the y-axis direction and graded in the x-axis directions by a constant factor of 0.95 (the element $\mathcal{E}$ is 0.0258×0.0101 in size). Mesh E is graded in both x- and y-axis directions by a constant factors of 0.95 and 1.1 in x- and y-directions, respectively (the element $\mathcal{E}$ is 0.0258×0.0466 in size).

In every case, the ability to cast $\tilde{\mathbf{G}}$ into the form dictated by the WBF assumption is excellent. Even for nonuniform meshes, with significant nonuniformities, the WBF assumption holds to within 0.08%. Therefore, the WBF assumption is embraced with a high degree of confidence.

Appendix B Ascertaining self force in PM schemes

To ascertain self force in a PM scheme, work through the four steps defining the PM scheme to determine what force is exerted on a single charge sitting on a mesh of infinite spatial extent and constant permittivity. Results for the NEC scheme will be derived, and the results for other schemes summarized.

Fig. 1 shows an element $\langle i,j\rangle$ and its immediate environment which establishes the necessary notation. Consider a line charge ρ_L located at (x,y) within element $\langle i,j\rangle$. The four steps of the NEC PM scheme proceed as follows:

1. *charge assignment to the mesh*: The charge assignment is parameterized by a vector of four charge weights $[c_{ij}\ c_{i+1,j}\ c_{i,j+1}\ c_{i+1,j+1}]^T \doteq \mathbf{c}$. The portion of the line charge ρ_L assigned to the four nodes is $\varrho = \rho_L \mathbf{c}$, where $\sum_{k,\ell} c_{k\ell} = 1$ by charge conservation, where $k = i, i+1$ and $\ell = j, j+1$. The four parameters are left unspecified for now.

2. *solve the Poisson equation*: Upon solving the Poisson equation on the infinite mesh, the potential of the nodes of element $\langle i,j\rangle$ can be written as $\varphi = \mathbf{G}\varrho$, where $\varphi = [\psi_{ij}\ \psi_{i+1,j}\ \psi_{i,j+1}\ \psi_{i+1,j+1}]^T$ is the vector of potential local to element $\langle i,j\rangle$ and $\mathbf{G} = (g_{ij})$ is a 4×4 matrix extracted from the inverse of the Laplacian on the infinite mesh. As discussed in Appendix A, adopting the WBF assumption dictates the matrix $\mathbf{G}$ has a special form, as shown in Eq. (9).

3. *compute forces on the mesh*: The NEC scheme requires the computation of four field values on the mesh; namely, $\Delta^x_{i+\frac{1}{2},j}$, $\Delta^x_{i+\frac{1}{2},j+1}$, $\Delta^y_{i,j+\frac{1}{2}}$ and $\Delta^y_{i+1,j+\frac{1}{2}}$ as defined in Eq. (2).

4. *interpolate to find force on the charge*: The interpolation scheme is parameterized by four interpolation coefficients $d_{i+\frac{1}{2},j}$, $d_{i+\frac{1}{2},j+1}$, $d_{i,j+\frac{1}{2}}$ and $d_{i+1,j+\frac{1}{2}}$, where $d_{i+\frac{1}{2},j} + d_{i+\frac{1}{2},j+1} = 1$ and $d_{i,j+\frac{1}{2}} + d_{i+1,j+\frac{1}{2}} = 1$. The field at the charge position (x,y), $\vec{E}(x,y) = [E^x; E^y]$, is given by $E^x = d_{i+\frac{1}{2},j}\Delta^x_{i+\frac{1}{2},j} + d_{i+\frac{1}{2},j+1}\Delta^x_{i+\frac{1}{2},j+1}$ and $E^y = d_{i,j+\frac{1}{2}}\Delta^y_{i,j+\frac{1}{2}} + d_{i+1,j+\frac{1}{2}}\Delta^y_{i+1,j+\frac{1}{2}}$.

To obtain zero self force, $\vec{E}(x,y) = \vec{0}$ is required; *i.e.*, $E^x = E^y = 0$. Setting $E^x = 0$, using the definition of differences from Eq. (2) and the values of $\psi_{k\ell}$ implied by $\varphi = \mathbf{G}\varrho = g_{11}\rho_L\tilde{\mathbf{G}}\mathbf{c}$ from Appendix A yields

$$\begin{aligned}
0 = E^x = [\; & d_{i+\frac{1}{2},j}(\psi_{ij} - \psi_{i+1,j}) + d_{i+\frac{1}{2},j+1}(\psi_{i,j+1} - \psi_{i+1,j+1})\;]/(x_{i+1} - x_i) = \\
& g_{11}\rho_L \;\{\; d_{i+\frac{1}{2},j} \quad [(1-\alpha)(c_{ij} - c_{i+1,j}) + (\beta-\gamma)(c_{i,j+1} - c_{i+1,j+1})] \quad + \\
& \qquad d_{i+\frac{1}{2},j+1} \quad [(\beta-\gamma)(c_{ij} - c_{i+1,j}) + (1-\alpha)(c_{i,j+1} - c_{i+1,j+1})] \quad \}/(x_{i+1} - x_i)\,.
\end{aligned} \tag{10}$$

Eq. (10) is the desired result, requiring only proper interpretation. What values for $c_{k\ell}$, $k = i, i+1$ and $\ell = j, j+1$, and $d_{i+\frac{1}{2},\ell}$, $\ell = j, j+1$ can be chosen in order to maintain $E^x = 0$ for any values of α, β and γ? Discarding immediately the degenerate solution $d_{i+\frac{1}{2},j} = d_{i+\frac{1}{2},j+1} = 0$, $E^x = 0$ is maintained if

$$c_{ij} = c_{i+1,j}; \quad c_{i,j+1} = c_{i+1,j+1}; \quad d_{i+\frac{1}{2},j} \text{ and } d_{i+\frac{1}{2},j+1} \text{ arbitrary.} \tag{11}$$

Performing an algebraic exercise analogous to that leading to Eq. (10) but beginning with the requirement $E^y = 0$ yields the following solution:

$$c_{ij} = c_{i,j+1}; \quad c_{i+1,j} = c_{i+1,j+1}; \quad d_{i,j+\frac{1}{2}} \text{ and } d_{i+1,j+\frac{1}{2}} \text{ arbitrary.} \tag{12}$$

Provided Eqs. (11) and (12) are obeyed, the NEC PM scheme will have zero self force. Taking Eqs. (11) and (12) together, and recalling that charge conservation dictates $\sum_{k,\ell} c_{k\ell} = 1$ for $k = i, i+1$ and $\ell = j, j+1$, the charge weights become $c_{ij} = c_{i+1,j} = c_{i,j+1} = c_{i+1,j+1} = \frac{1}{4}$. Recalling the summing properties of the interpolation coefficients from step 4 above, the four interpolation coefficients are set (quite arbitrarily, really!) to $d_{i+\frac{1}{2},j} = d_{i+\frac{1}{2},j+1} = \frac{1}{2}$ and $d_{i,j+\frac{1}{2}} = d_{i+1,j+\frac{1}{2}} = \frac{1}{2}$. This concludes the NEC PM scheme derivation.

The results of similar algebraic investigations to ascertain the self force in CIC and mixed NGP–CIC schemes are now summarized. The CIC scheme uses four charge weights c_{ij},

$c_{i+1,j}$, $c_{i,j+1}$ and $c_{i+1,j+1}$, as well as four force interpolation coefficients d_{ij}, $d_{i+1,j}$, $d_{i,j+1}$ and $d_{i+1,j+1}$, both sets associated with the nodes of element $\langle i,j\rangle$. Zero self force is maintained in the x-axis direction ($E^x = 0$) when

$$\begin{aligned} c_{i+1,j}d_{ij} - c_{ij}d_{i+1,j} + c_{i+1,j+1}d_{i,j+1} - c_{i,j+1}d_{i+1,j+1} = 0\,; \\ c_{i+1,j}d_{i,j+1} - c_{i,j+1}d_{i+1,j} + c_{i+1,j+1}d_{ij} - c_{ij}d_{i+1,j+1} = 0\,. \end{aligned} \tag{13}$$

Zero self force is maintained in the y-axis direction ($E^y = 0$) when

$$\begin{aligned} c_{i,j+1}d_{ij} - c_{ij}d_{i,j+1} + c_{i+1,j+1}d_{i+1,j} - c_{i+1,j}d_{i+1,j+1} = 0\,; \\ c_{i,j+1}d_{i+1,j} - c_{i+1,j}d_{i,j+1} + c_{i+1,j+1}d_{ij} - c_{ij}d_{i+1,j+1} = 0\,. \end{aligned} \tag{14}$$

Both Eqs. (13) and (14) are solved when $c_{k\ell} = d_{k\ell}$, $k = i, i+1$ and $\ell = j, j+1$, *i.e.*, when the same charge weightings and force interpolations are used. This is in agreement with Ref. [1], although shown in a very different way. These coefficients are chosen according to spatial interpolation considerations as the values given in step 1 of Sec. 3.

The NEC-x–CIC*-y scheme maintains zero self force in the x-axis direction ($E^x = 0$) when Eq. (11) is obeyed, and in the y-axis direction ($E^y = 0$) when Eq. (14) is obeyed. For NEC-y–CIC*-x, Eq. (12) and (13) must be obeyed. The descriptions of the schemes in Sec. 3 satisfy the relevant equations as required.

Appendix C Taxonomy of NEC and NEC–CIC* Schemes

In Sec. 5-3-4 of Ref. [1], the authors discuss a hierarchy of charge assignment schemes. As part of this discussion, the cloud shape function S and charge assignment function W are defined. For completeness, S and W are given for the NEC and NEC–CIC* schemes. There are two caveats: (i) these functions are only definable on tensor-product meshes with uniform mesh spacing in each axis direction, and (ii) these functions only apply to the charge assignment step, and *not* to the force interpolation step. For simplicity, these functions are given here with a uniform mesh spacing h in both axis direction. For the NEC scheme:

$$S(x,y) \;=\; \frac{1}{4}\,[\;\delta(x-\frac{h}{2})\delta(y-\frac{h}{2}) + \delta(x-\frac{h}{2})\delta(y+\frac{h}{2}) +$$

$$
\begin{aligned}
& \delta(x+\frac{h}{2})\delta(y-\frac{h}{2})+\delta(x+\frac{h}{2})\delta(y+\frac{h}{2})\,]\;, \\
W(x,y) &= \frac{1}{4}\,\Pi(\frac{x}{2h})\;\wedge(\frac{y}{2h})\,; \qquad (15)
\end{aligned}
$$

for the NEC-x–CIC*-y scheme:

$$
\begin{aligned}
S(x,y) &= \frac{1}{2h}\left[\delta(x-\frac{h}{2})+\delta(x+\frac{h}{2})\right]\;\Pi(\frac{y}{h})\,, \\
W(x,y) &= \frac{1}{2}\,\Pi(\frac{x}{2h})\;\wedge(\frac{y}{h})\,; \qquad (16)
\end{aligned}
$$

and for the NEC-y–CIC*-x scheme:

$$
\begin{aligned}
S(x,y) &= \frac{1}{2h}\,\Pi(\frac{x}{h})\;\left[\delta(y-\frac{h}{2})+\delta(y+\frac{h}{2})\right]\,, \\
W(x,y) &= \frac{1}{2}\;\wedge(\frac{x}{h})\;\Pi(\frac{y}{2h})\,; \qquad (17)
\end{aligned}
$$

where the functions Π and $\wedge$ are the "top-hat" and "triangle" functions of Ref. [1].

Fig. 10 and Fig. 11 depict the cloud-shape and charge assignment functions for the NEC, NEC-x–CIC*-y and NEC-y–CIC*-x schemes proposed here, and also for the CIC scheme for comparison.

References

[1] R. Hockney and J. Eastwood, *Computer Simulation Using Particles.* New York: Adam Hilger, 1988.

[2] P. Lugli and D. Ferry, "Dynamical screening of hot carriers in semiconductors from a coupled molecular-dynamics and ensemble Monte Carlo simulation," *Phys. Rev. Lett.*, vol. 56, no. 12, pp. 1295–1297, 1986.

[3] L. Greengard and M. Moura, "On the numerical evaluation of electrostatic fields in composite materials," *Acta Numerica*, pp. 379–410, 1994.

[4] K. Throngnumchai, K. Asada, and T. Sugano, "Modeling of 0.1-μm MOSFET on SOI structure using Monte Carlo simulation technique," *IEEE Trans. Electron Devices*, vol. 33, no. 7, pp. 1005–1011, 1986.

[5] J. Higman, K. Hess, C. Hwang, and R. Dutton, "Coupled Monte Carlo–drift diffusion analysis of hot-electron effects in MOSFET's," *IEEE Trans. Electron Devices*, vol. 36, no. 5, pp. 930–937, 1989.

[6] M. Fischetti and S. Laux, "Monte Carlo analysis of electron transport in small semiconductor devices including band-structure and space-charge effects," *Phys. Rev. B*, vol. 38, no. 14, pp. 9721–9745, 1988.

[7] M. Fischetti and S. Laux, “DAMOCLES theoretical manual version 0.2.” unpublished, April 1995.

[8] J. Jackson, *Classical Electrodynamics.* New York: John Wiley and Sons, second ed., 1975.

[9] P. Degond, F. Hermeline, P. Raviart, and J. Segré, “Numerical modeling of axisymmetric electron beam devices using a coupled particle-finite element method,” *IEEE Trans. Magn.*, vol. 27, no. 5, pp. 4177–4180, 1991.

[10] M. Matsumoto and S. Kawata, “TRIPIC: Triangular-mesh particle-in-cell code,” *J. Comput. Phys.*, vol. 87, no. 2, pp. 488–493, 1990.

[11] R. Assous, P. Degond, and J. Segré, “A particle-tracking method for 3d electromagnetic PIC codes on unstructured meshes,” *Comput. Phys. Commun.*, vol. 72, no. 2-3, pp. 105–114, 1992.

[12] O. Zienkiewicz, *The Finite Element Method.* New York: McGraw-Hill, third ed., 1977.

Mesh	$\tilde{\mathbf{G}}$ matrix values α	β	γ	diagonal
A	0.94384 ± 0.00095	0.94384 ± 0.00095	0.92849 ± 0.00001	1.00000 ± 0.00191
B	0.95013 ± 0.00098	0.94122 ± 0.00005	0.93018 ± 0.00001	1.00000 ± 0.00504
C	0.93192 ± 0.00099	0.94810 ± 0.00116	0.92245 ± 0.00002	1.00000 ± 0.00542
D	0.91418 ± 0.00118	0.95784 ± 0.00328	0.90997 ± 0.00004	1.00000 ± 0.00528
E	0.94537 ± 0.00543	0.91528 ± 0.00316	0.90721 ± 0.00020	1.00000 ± 0.00759

Table 1: $\tilde{\mathbf{G}}$ matrix values for five meshes; only mesh A is uniform in both x- and y-directions.

FIGURE CAPTIONS

Fig. 1 A portion of a two-dimensional tensor-product mesh in the vicinity of element $\langle i, j \rangle$ illustrating the meshlines x_ℓ and y_ℓ, and the piecewise constant permittivities $\epsilon_{k\ell}$. The mesh locations where charge density and potential reside are element nodes; for the central element $\langle i, j \rangle$, these are indicated by solid dots. The open dots indicate element edge midpoints for element $\langle i, j \rangle$.

Fig. 2 Force on a single plane of charge $\rho_A = -2 \times 10^{12}\,\mathrm{cm}^{-2}$ versus position of that charge within a one-dimensional model problem described in the text. Five such plots of force versus position are shown, each vertically displaced from the other as indicated by the dotted baselines corresponding to a zero force value. The uniform mesh spacing is indicated by the vertical marks along the bottom edge of the figure; there are 21 nodes and 20 intervals in the mesh. The curve marked "EXACT" is an exact analytical solution to the model problem; all other curves are for PM schemes discussed in the text.

Fig. 3 Same as in Fig. 2, except that the various PM coupling schemes are exercised on a nonuniformly spaced mesh. The nonuniform mesh spacing is indicated by the vertical marks along the bottom edge of the figure; there are 24 nodes and 23 intervals in the mesh.

Fig. 4 The x-directed force on a single line charge $\rho_L = -1.2 \times 10^6\,\mathrm{cm}^{-1}$ versus position along path 1 of that charge within a two-dimensional model problem described in the text. Five such plots of force versus position are shown, each vertically displaced from the other as indicated by the dotted baselines corresponding to a zero force value. These calculations were performed on a 25×25 uniform mesh; where path 1 crosses x- and y-meshlines is indicated by the upper and lower row of vertical marks along the bottom of the figure, respectively. All curves are for PM schemes exercised on this mesh except the curve marked "EXACT", which is a computation performed on a highly refined mesh.

Fig. 5 Same as Fig. 4, except the y-directed force on the line charge is shown.

Fig. 6 Same as Fig. 4, except the line charge moves along path 2.

Fig. 7 Same as Fig. 4, except the y-directed force on the line charge is shown and the charge moves along path 2.

Fig. 8 The magnitude of the force on a single line charge $\rho_L = -1.2 \times 10^6\,\mathrm{cm}^{-1}$ versus position along path 2 of that charge within a two-dimensional model problem described in the text. Five such plots of force versus position are shown, each vertically displaced from the other as indicated by the dotted baselines corresponding to a zero force value. These calculations were performed on a 25×25 nonuniform mesh; where path 2 crosses x- and y-meshlines is indicated by the upper and lower row of vertical marks along the bottom of the figure, respectively. All curves are for PM schemes exercised on this mesh except the curve marked "EXACT", which is a computation performed on a highly refined mesh.

Fig. 9 Contours of the y-directed force on a line charge $\rho_L = -1.2 \times 10^6\,\mathrm{cm}^{-1}$ for the two-dimensional model problem posed on a uniform mesh, computed with the CIC* scheme. The force at location (x, y) is that force exerted on ρ_L when it is located at (x, y). Only a subregion of the entire two-dimensional model problem domain is shown. The portions of path 1 and 2 within the subregion are shown as dashed lines.

Fig. 10 Cloud-shape functions $S(x, y)$, as defined in Ref. [1], for four PM schemes on a uniform tensor-product mesh of mesh spacing h: (a) CIC or CIC*, (b) NEC, (c) NEC-x–CIC*-y and (d) NEC-y–CIC*-x.

Fig. 11 Charge assignment functions $W(x, y)$, as defined in Ref. [1], for four PM schemes on a uniform tensor-product mesh of mesh spacing h: (a) CIC or CIC*, (b) NEC, (c) NEC-x–CIC*-y and (d) NEC-y–CIC*-x.

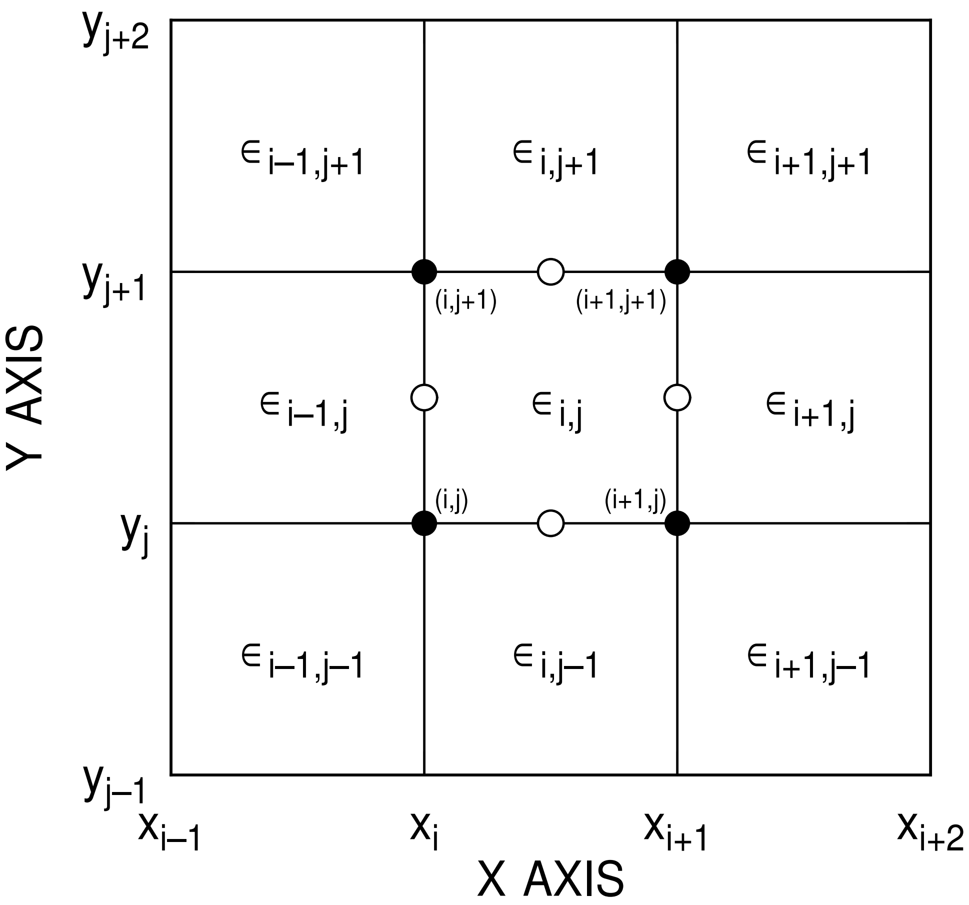

Figure 1: A portion of a two-dimensional tensor-product mesh in the vicinity of element $\langle i,j\rangle$ illustrating the meshlines x_ℓ and y_ℓ, and the piecewise constant permittivities $\epsilon_{k\ell}$. The mesh locations where charge density and potential reside are element nodes; for the central element $\langle i,j\rangle$, these are indicated by solid dots. The open dots indicate element edge midpoints for element $\langle i,j\rangle$.

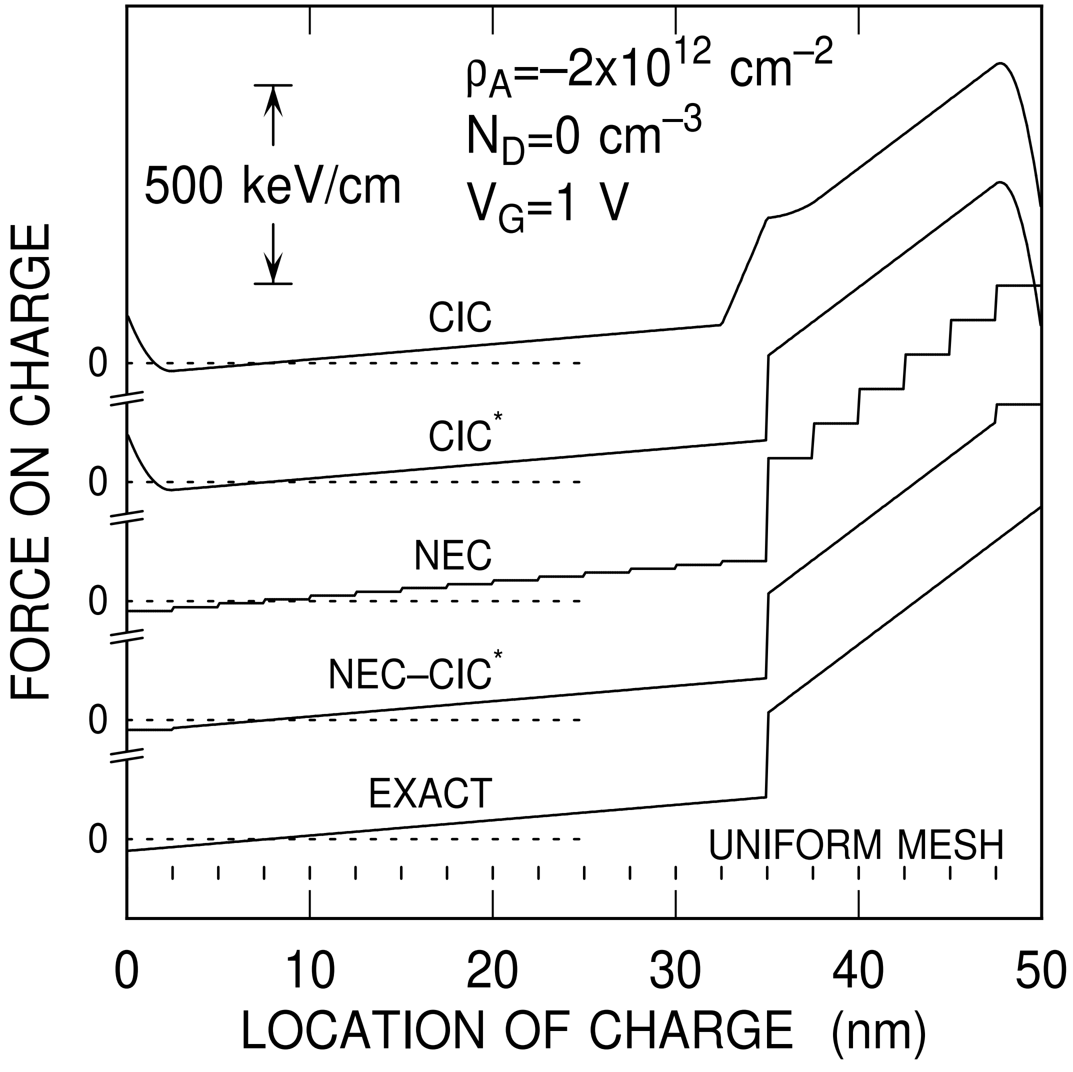

Figure 2: Force on a single plane of charge $\rho_A = -2 \times 10^{12}\,\mathrm{cm}^{-2}$ versus position of that charge within a one-dimensional model problem described in the text. Five such plots of force versus position are shown, each vertically displaced from the other as indicated by the dotted baselines corresponding to a zero force value. The uniform mesh spacing is indicated by the vertical marks along the bottom edge of the figure; there are 21 nodes and 20 intervals in the mesh. The curve marked "EXACT" is an exact analytical solution to the model problem; all other curves are for PM schemes discussed in the text.

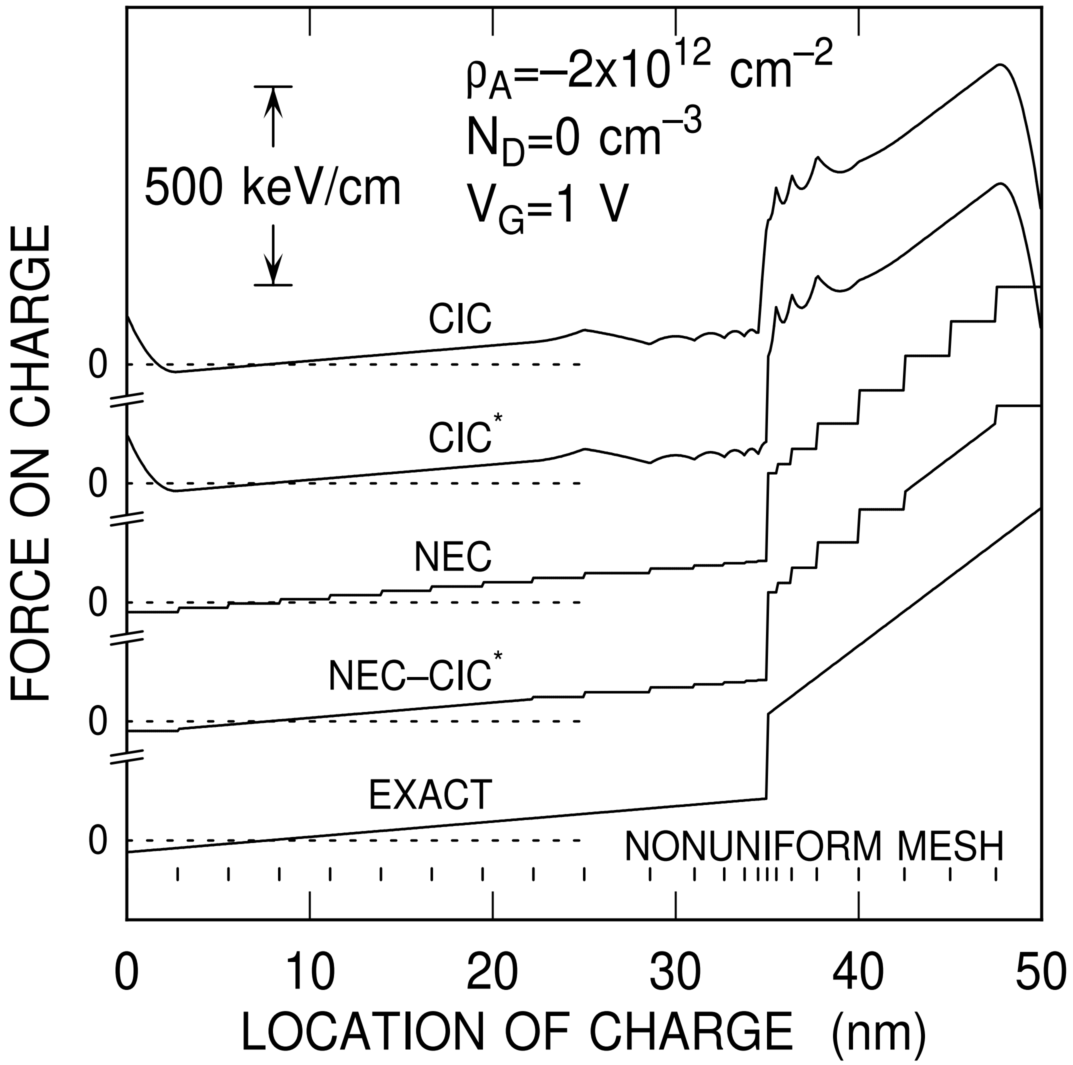

Figure 3: Same as in Fig. 2, except that the various PM coupling schemes are exercised on a nonuniformly spaced mesh. The nonuniform mesh spacing is indicated by the vertical marks along the bottom edge of the figure; there are 24 nodes and 23 intervals in the mesh.

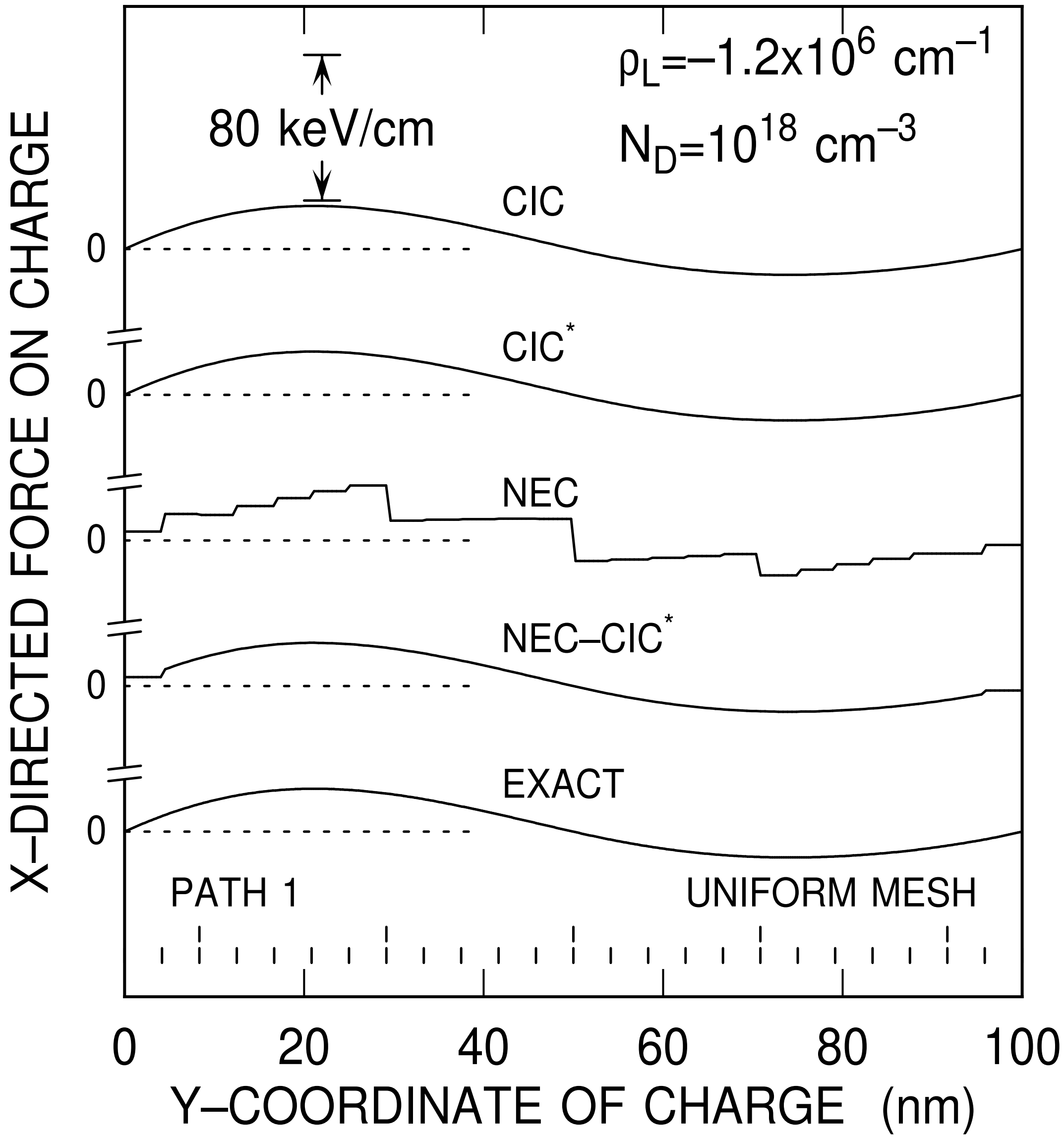

Figure 4: The x-directed force on a single line charge $\rho_L = -1.2 \times 10^6\,\mathrm{cm}^{-1}$ versus position along path 1 of that charge within a two-dimensional model problem described in the text. Five such plots of force versus position are shown, each vertically displaced from the other as indicated by the dotted baselines corresponding to a zero force value. These calculations were performed on a 25×25 uniform mesh; where path 1 crosses x- and y-meshlines is indicated by the upper and lower row of vertical marks along the bottom of the figure, respectively. All curves are for PM schemes exercised on this mesh except the curve marked "EXACT", which is a computation performed on a highly refined mesh.

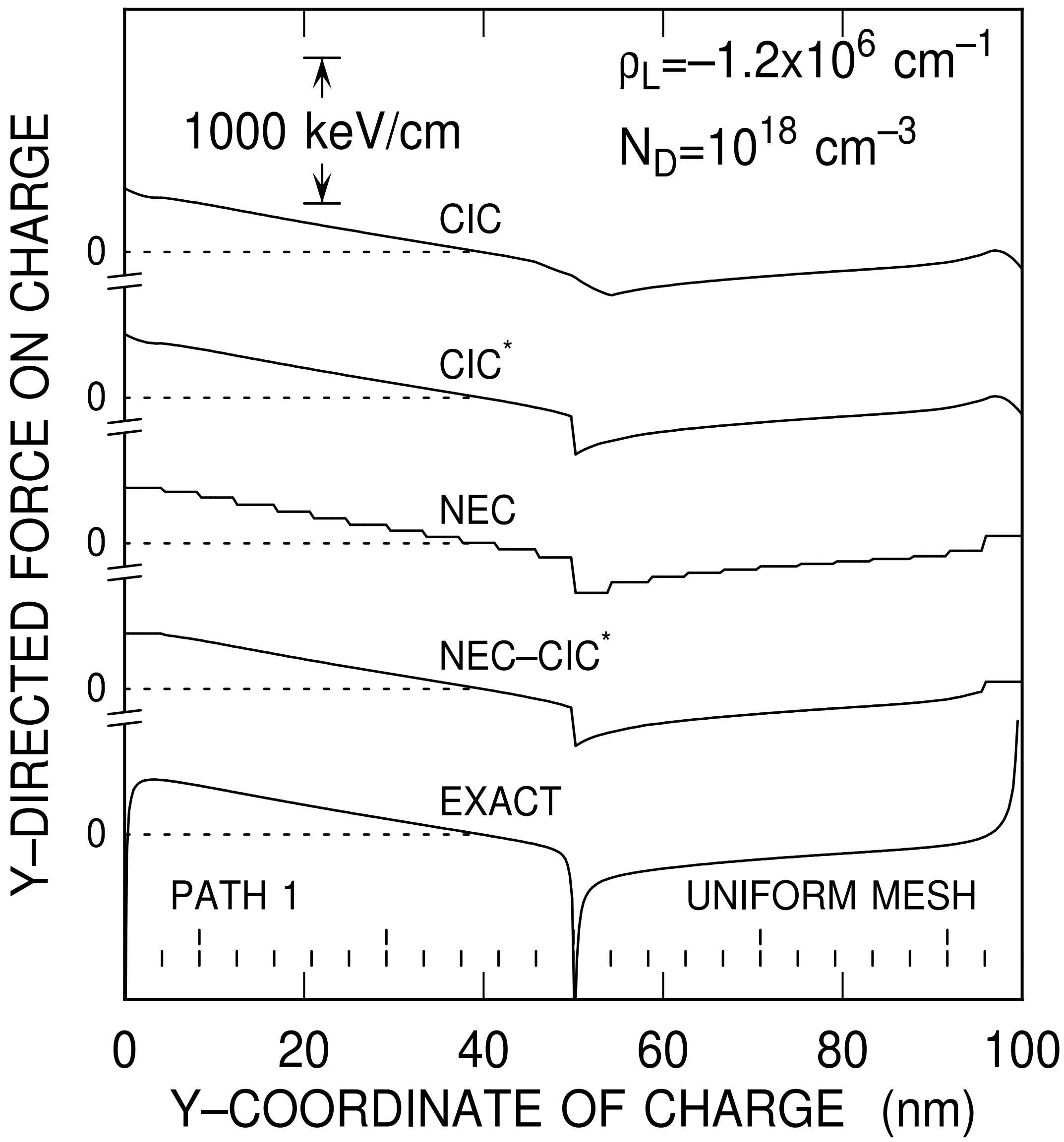

Figure 5: Same as Fig. 4, except the y-directed force on the line charge is shown.

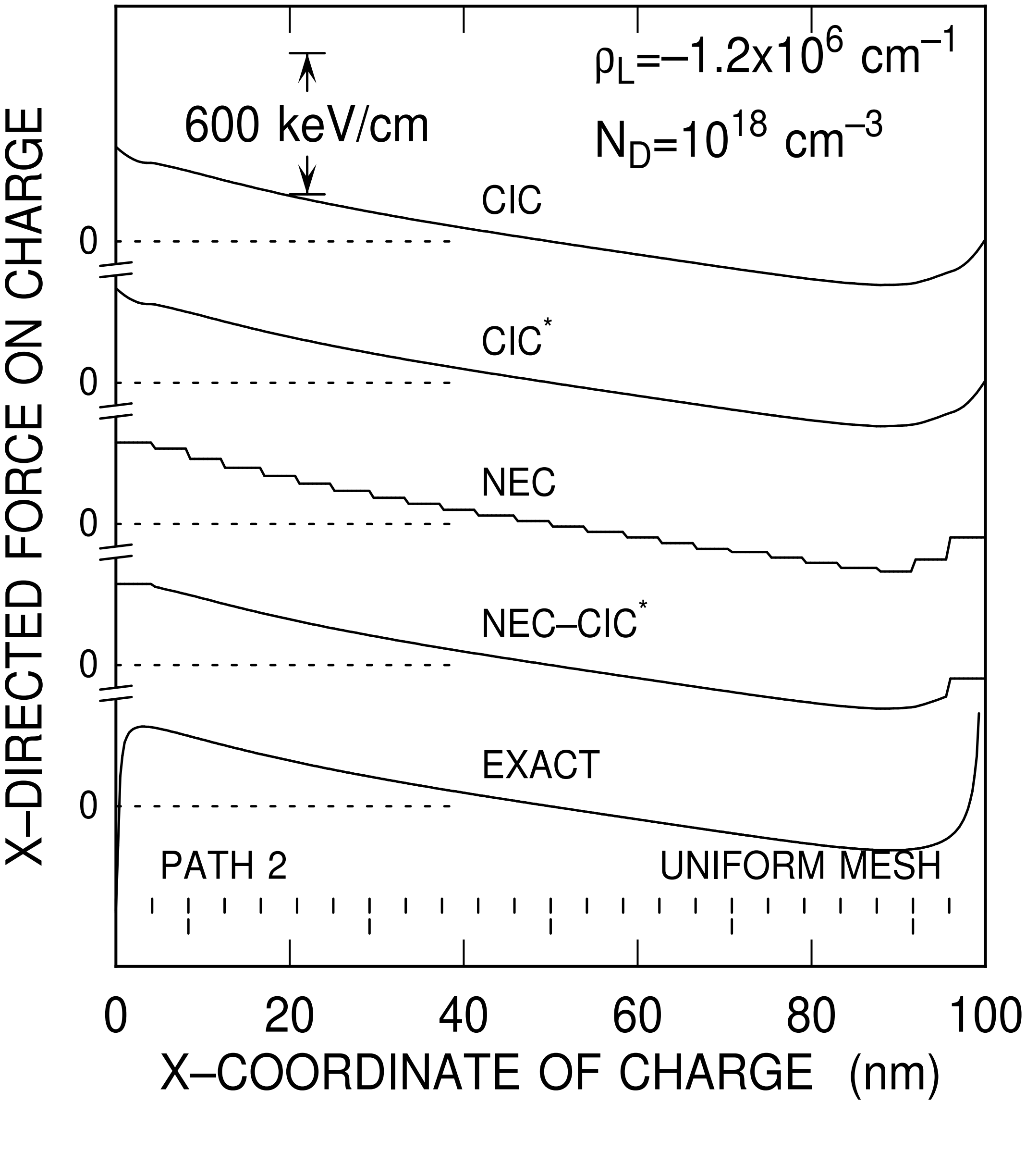

Figure 6: Same as Fig. 4, except the line charge moves along path 2.

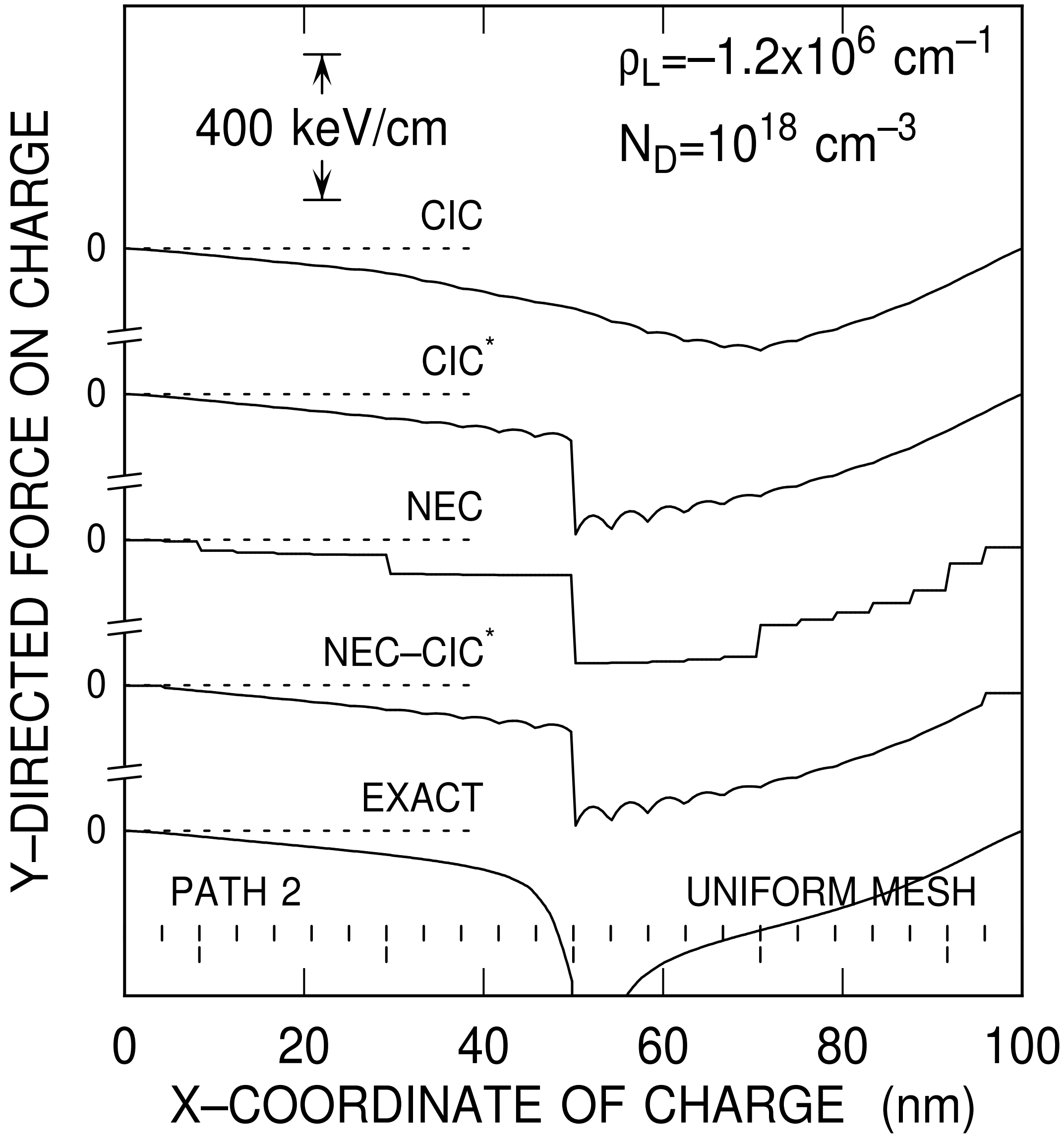

Figure 7: Same as Fig. 4, except the y-directed force on the line charge is shown and the charge moves along path 2.

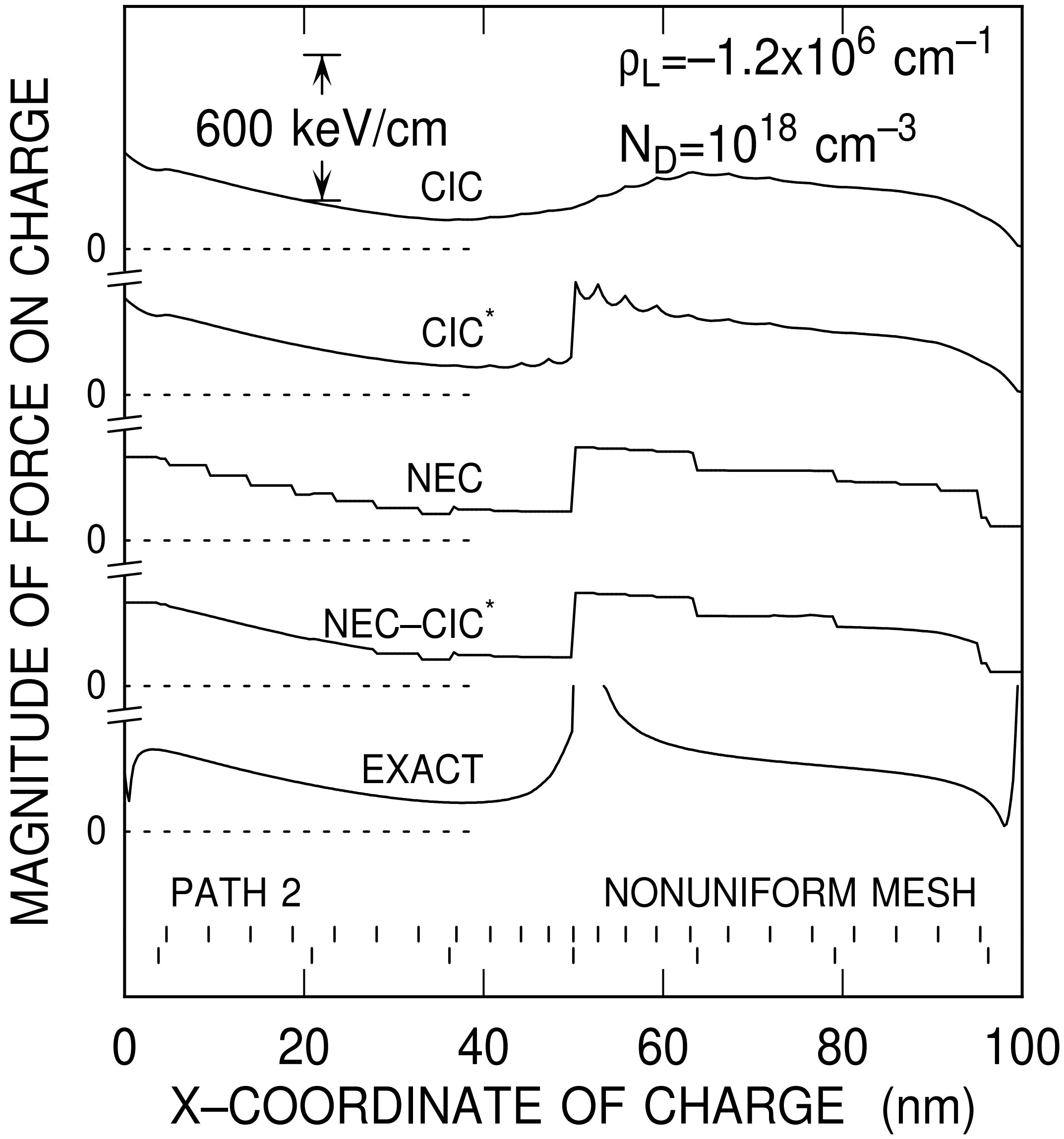

Figure 8: The magnitude of the force on a single line charge $\rho_L = -1.2 \times 10^6\,\mathrm{cm}^{-1}$ versus position along path 2 of that charge within a two-dimensional model problem described in the text. Five such plots of force versus position are shown, each vertically displaced from the other as indicated by the dotted baselines corresponding to a zero force value. These calculations were performed on a 25×25 nonuniform mesh; where path 2 crosses x- and y-meshlines is indicated by the upper and lower row of vertical marks along the bottom of the figure, respectively. All curves are for PM schemes exercised on this mesh except the curve marked "EXACT", which is a computation performed on a highly refined mesh.

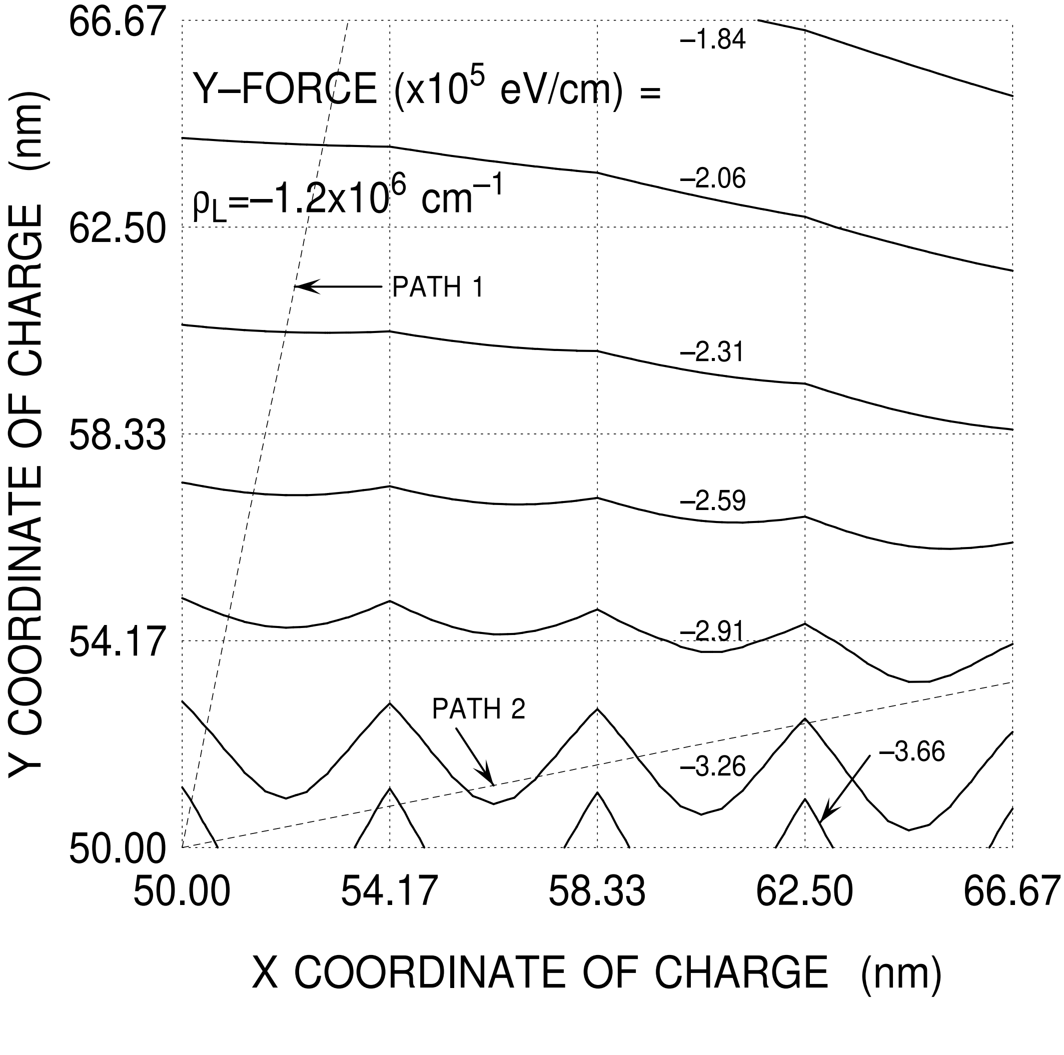

Figure 9: Contours of the y-directed force on a line charge $\rho_L = -1.2 \times 10^6\,\mathrm{cm}^{-1}$ for the two-dimensional model problem posed on a uniform mesh, computed with the CIC* scheme. The force at location (x, y) is that force exerted on ρ_L when it is located at (x, y). Only a subregion of the entire two-dimensional model problem domain is shown. The portions of path 1 and 2 within the subregion are shown as dashed lines.

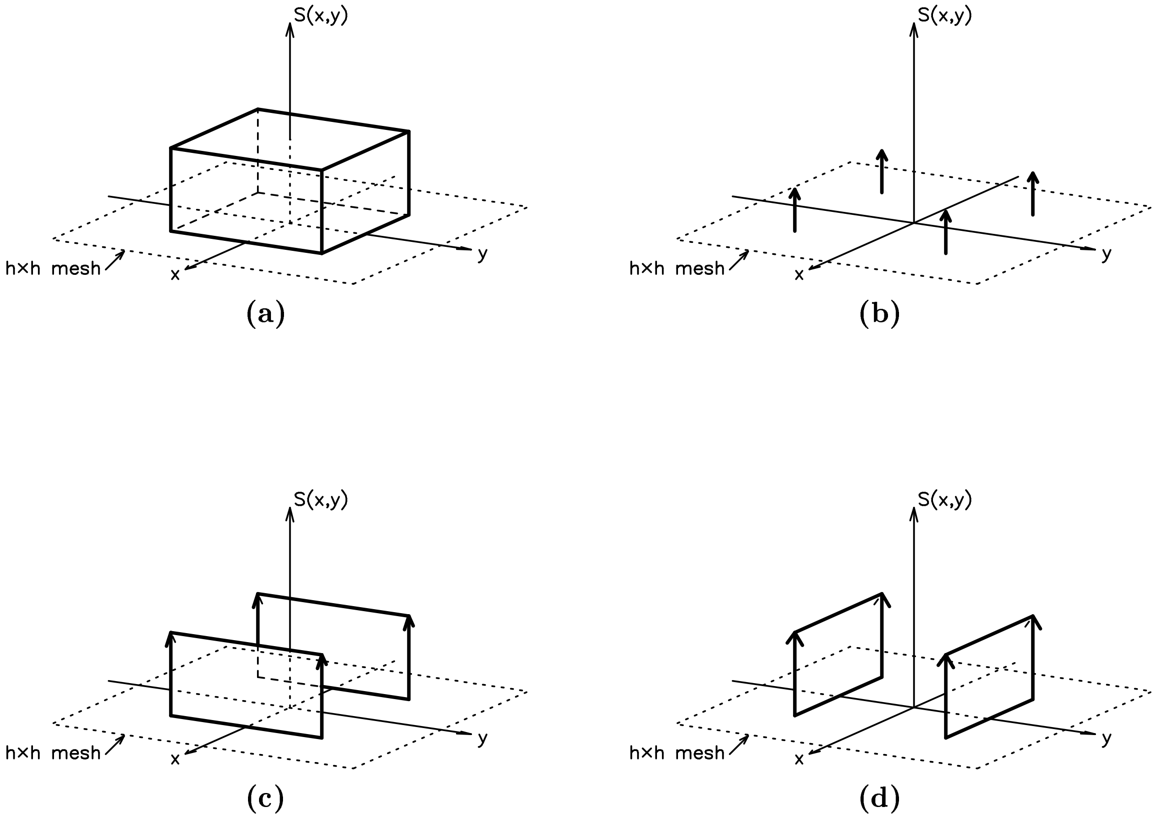

Figure 10: Cloud-shape functions $S(x, y)$, as defined in Ref. [1], for four PM schemes on a uniform tensor-product mesh of mesh spacing h: (a) CIC or CIC*, (b) NEC, (c) NEC-x–CIC*-y and (d) NEC-y–CIC*-x.

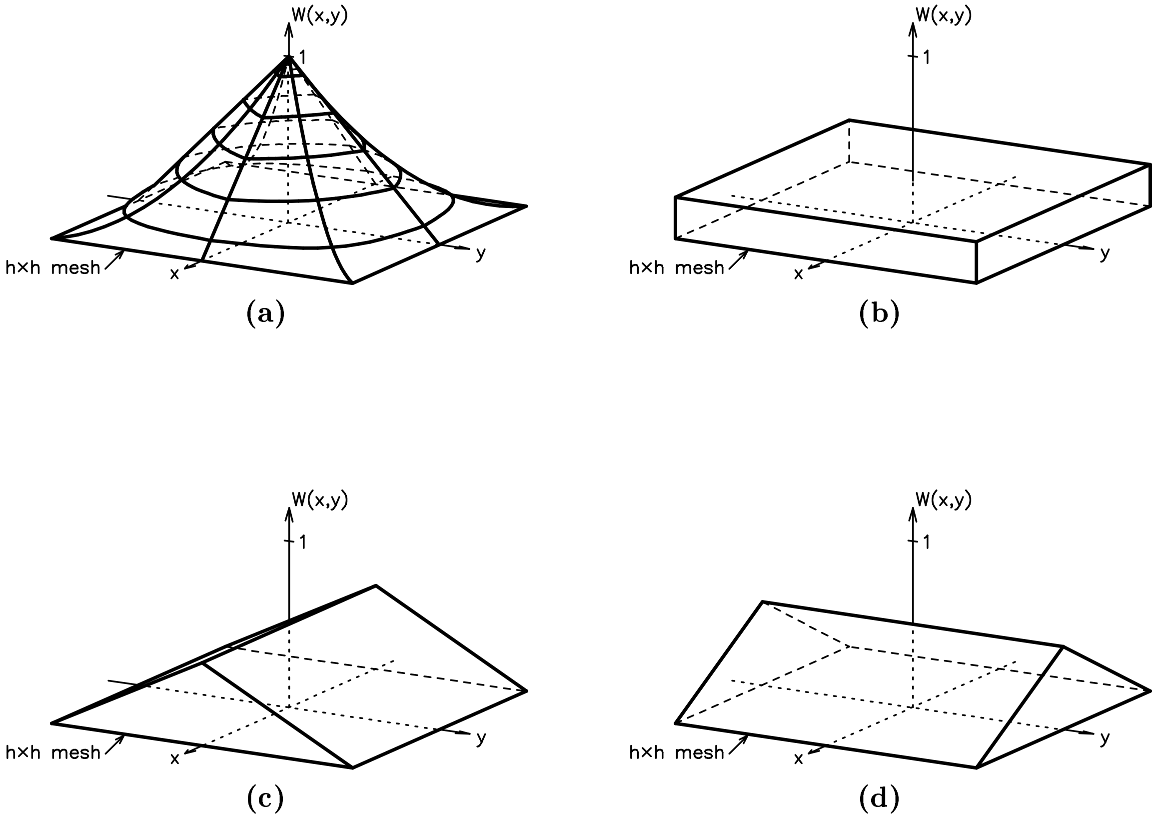

Figure 11: Charge assignment functions $W(x, y)$, as defined in Ref. [1], for four PM schemes on a uniform tensor-product mesh of mesh spacing h: (a) CIC or CIC*, (b) NEC, (c) NEC-x–CIC*-y and (d) NEC-y–CIC*-x.